สมบัติทางความร้อนและทางกลของวัสดุประกอบแต่งจากระบบสารเติมปริมาณสูง อลูมินา-พอลิเบนซอกซาซีน

นายจิรวัฒน์ ขจรไชยกูล

วิทยานิพนธ์นี้เป็นส่วนหนึ่งของการศึกษาตามหลักสูตรปริญญาวิศวกรรมศาสตรมหาบัณฑิต
สาขาวิชาวิศวกรรมเคมี ภาควิชาวิศวกรรมเคมี
คณะวิศวกรรมศาสตร์ จุฬาลงกรณ์มหาวิทยาลัย
ปีการศึกษา 2555

THERMAL AND MECHANICAL PROPERTIES OF HIGHLY-FILLED ALUMINA-POLYBENZOXAZINE COMPOSITES

Mr. Jirawat Kajohnchaiyagual

A Thesis Submitted in Partial Fulfillment of the Requirements
for the Degree of Master of Engineering Program in Chemical Engineering
Department of Chemical Engineering
Faculty of Engineering
Chulalongkorn University
Academic Year 2012

Thesis Title	THERMAL AND MECHANICAL PROPERTIES OF HIGHLY-FILLED ALUMINA-POLYBENZOXAZINE COMPOSITES
By	Mr. Jirawat Kajohnchaiyagual
Field of Study	Chemical Engineering
Thesis Advisor	Associate Professor Sarawut Rimdusit, Ph.D.
Thesis Co-advisor	Chanchira Jubsilp, D.Eng.

Accepted by the Faculty of Engineering, Chulalongkorn University in Partial Fulfillment of the Requirements for the Master's Degree

.....Dean of the Faculty of Engineering
(Associate Professor Boonsom Lerdhirunwong, Dr.Ing.)

THESIS COMMITTEE

.....Chairman
(Professor Suttichai Assabumrungrat, Ph.D.)

.....Thesis Advisor
(Associate Professor Sarawut Rimdusit, Ph.D.)

.....Thesis Co-advisor
(Chanchira Jubsilp, D.Eng)

.....Examiner
(Associate Professor Siriporn Damrongsakkul, Ph.D.)

.....External Examiner
(Associate Professor Chirakarn Muangnapoh, Dr.Ing.)

จิรวัฒน์ ขจรไชยกูล : สมบัติทางความร้อนและทางกลของวัสดุประกอบแต่งจากระบบสารเติมปริมาณสูงอลูมินา-พอลิเบนซอกซาซีน (THERMAL AND MECHANICAL PROPERTIES OF HIGHLY–FILLED ALUMINA-POLYBENZOXAZINE COMPOSITES) อ. ที่ปรึกษาวิทยานิพนธ์หลัก : รศ. ดร. ศราวุธ ริมดุสิต, อ. ที่ปรึกษาวิทยานิพนธ์ร่วม : ดร. จันจิรา จับศิลป์, 91 หน้า.

งานวิจัยนี้มีวัตถุประสงค์เพื่อศึกษา สมบัติทางความร้อนและสมบัติทางกลในระบบสารเติมปริมาณสูงของพอลิเมอร์คอมพอสิทที่ใช้พอลิเบนซอกซาซีนเป็นตัวเมทริกซ์และสารเติมเป็นอลูมินา สภาวะที่ใช้ในการอัดขึ้นรูปพอลิเบนซอกซาซีนคอมพอสิทที่เติมด้วยอลูมินาปริมาณสูงข้างต้นคือที่ อุณหภูมิ 200 องศาเซลเซียส และความดันในการอัดขึ้นรูปเท่ากับ15 เมกะปาสคาล เป็นเวลา 2 ชั่วโมง เพื่อให้คอมพอสิทที่ได้มีการบ่มตัวสมบูรณ์ ปริมาณของอลูมินาที่เติมลงไปในคอมพอสิทอยู่ระหว่าง 50 ถึง 83 เปอร์เซ็นต์โดยน้ำหนัก โดยพบว่าค่าความหนาแน่นของคอมพอสิทที่ได้จะอยู่ในช่วง 1.19-2.811 กรัมต่อลูกบาศก์เซนติเมตร ซึ่งเป็นไปตามกฎการผสม นอกจากนี้จากการทดลองพบว่าปริมาณสูงสุดของอลูมินาที่เติมได้ในพอลิเบนซอกซาซีนอยู่ที่ 83 เปอร์เซ็นต์โดยน้ำหนัก หรือ 60 เปอร์เซ็นโดยปริมาตร ซึ่งที่ระดับการเติมสูงสุดนี้พบว่าค่ามอดูลัสสะสมที่อุณหภูมิห้อง มีค่าสูงถึง 45.3 จิกะปาสคาล ซึ่งเพิ่มขึ้นจากมอดูลัสสะสมของพอลิเบนซอกซาซีนที่มีค่าเท่ากับ 5.9 จิกะปาสคาล ถึงประมาณ 600 เปอร์เซนต์ อุณหภูมิการเปลี่ยนสถานะคล้ายแก้ว (T_g) ของคอมพอสิทที่ได้มีค่าอยู่ระหว่าง 178 ถึง 188 องศาเซลเซียส ซึ่งค่าเพิ่มขึ้นตามปริมาณอลูมินาที่เพิ่มสูงขึ้น ส่วนอุณหภูมิการสลายตัวทางความร้อนของคอมพอสิทที่ได้มีค่าอยู่ระหว่าง 336 ถึง 389 องศาเซลเซียส ซึ่งค่าเพิ่มขึ้นตามปริมาณอลูมินาที่เพิ่มสูงขึ้นเช่นเดียวกัน นอกจากนี้ยังพบว่าค่ามอดูลัสและความแข็งแรงภายใต้แรงดัดโค้งที่ปริมาณอลูมินาสูงสุด 83 เปอร์เซ็นต์โดยน้ำหนักมีค่าเท่ากับ 36.4 จิกะปาสคาลและ 142.42 เมกะปาสคาลตามลำดับ และยังมีความความแข็งสูงถึง 1124 เมกะปาสคาลอีกด้วย ส่วนค่าการดูดซึมของน้ำของระบบสารเติมนี้พบว่ามีค่าค่อนข้างต่ำ โดยมีค่าประมาณ 0.054 เปอร์เซ็นต์ ที่เวลาทดสอบ 24 ชั่วโมง จากสมบัติดังกล่าวข้างต้นของคอมพอสิทระหว่างพอลิเบนซอกซาซีนกับอลูมินาพบว่ามีความเหมาะสมสำหรับประยุกต์ใช้ในงานต้านทานรอยขีดข่วน ทนการสึกหรอ รวมถึงงานในด้านอิเล็กทรอนิกส์

ภาควิชา วิศวกรรมเคมี ลายมือชื่อนิสิต .....

สาขาวิชา วิศวกรรมเคมี ลายมือชื่อ อ.ที่ปรึกษาวิทยานิพนธ์หลัก .....

สาขาวิชา วิศวกรรมเคมี ลายมือชื่อ อ.ที่ปรึกษาวิทยานิพนธ์ร่วม .....

ปีการศึกษา 2555

5470504221: MAJOR CHEMICAL ENGINEERING
KEYWORDS: POLYMERCOMPOSITE/ ALUMINA / HIGHLY FILLED / POLYBENZOXAZINE / MECHANICAL PROPERTIES / THERMAL PROPERTIES

JIRAWAT KAJOHNCHAIYAGUAL: THERMAL AND MECHANICAL PROPERTIES OF HIGHLY–FILLED ALUMINA-POLYBENZOXAZINE COMPOSITES.
ADVISOR: ASSOC. PROF. SARAWUT RIMDUSIT, Ph.D.,
CO-ADVISOR: CHANCHIRA JUBSILP, D.Eng, 91 pp.

This research aims to study thermal and mechanical properties of highly filled alumina composites utilizing polybenzoxazine as a matrix. The condition for the compression molding to produce highly filled alumina-polybenzoxazine composites was at the temperature of 200^{o}C, and the pressure of 15 MPa in a hydraulic hot-press machine for 2 hours to assure a fully cured specimen. The composition of alumina filler was achieved to be in the range of 50 to 83% by weight. The densities of the obtained composites were found to be in a range of 1.19-2.811 g/cm^{3} as predicted by rule of mixture. The experimental results revealed that at the maximum alumina content of 83wt% or 60vol% filled in the polybenzoxazine, storage modulus at room temperature of the specimen was raised from 5.9 GPa of the neat polybenzoxazine up to about 45.3 GPa in the composites which is about 600% improvement. The glass-transition temperatures (T_g) of the prepared composites were observed to be ranging from 178 to 188^{o}C and the values substantially increased with increasing the alumina contents. The degradation temperature (T_d) of the prepared composites were observed to be ranging from 336 to 389^{o}C. Furthermore, at alumina content of 83wt% in the polybenzoxazine, the composite's flexural modulus and flexural strength were found to be as high as 36.4 GPa and 142.42 MPa, respectively, whereas the Vickers hardness was determined to be as high as 1124 MPa. Water absorption of this filled system was relatively low with the value of about 0.054% at 24 hours. Consequently, the data on thermal properties and mechanical properties of the alumina filled polybenzoxazine composites are highly attractive for wear resistance and electronic applications.

Department: Chemical Engineering Student's Signature .....
Field of Study: Chemical Engineering Advisor's Signature .....
Field of Study: Chemical Engineering Co-advisor's Signature .....
Academic Year 2012

ACKNOWLEDGEMENTS

I would like to express my sincerest gratitude and deep appreciation to my advisor, Assoc. Prof. Dr. Sarawut Rimdusit and my co-advisor, Dr. Chanchira Jubsilp with their kindness, invaluable supervision, guidance, advice, and encouragement throughout the course of this study.

I also gratefully thank Prof. Dr. Suttichai Assabumrungrat, Assoc. Prof. Dr. Siriporn Damrongsakkul, and Assoc. Prof. Dr. Chirakarn Muangnapoh for their invaluable comments as a thesis committee.

In addition, I would like to acknowledge the financial supports from the higher Education Research Promotion, HERP (Project No. 054628), the Higher Education Research Promotion and National Research University Project of Thailand, Office of the Higher Education Commission (AM1076A), and 100th Anniversary of Chulalongkorn University Academic Funding through Ratchadapiseksomphot Endowment Fund, CU. Bisphenol A is kindly supported by Thai Polycarbonate Co., Ltd. (TPCC).

Additionally, I would like to thank all members of Polymer Engineering Laboratory of the Department of Chemical Engineering, Faculty of Engineering, Chulalongkorn University, for their assistance, discussion, and friendly encouragement in solving problems. Finally, my deepest regards to my family, particularly my parents, who have always been the source of my unconditional love, understanding, and generous encouragement during my studies. Also, every person who deserves thanks for encouragement and support that cannot be listed.

CONTENTS

PAGE

CHAPTER **PAGE**

CHAPTER **PAGE**

LIST OF TABLES

TABLE **PAGE**

LIST OF FIGURES

FIGURE **PAGE**

FIGURE **PAGE**

FIGURE **PAGE**

FIGURE **PAGE**

CHAPTER I

INTRODUCTION

1.1Overview

Nowadays, ceramics like alumina, silicon carbide, and silicon oxide have been used in many engineering applications such as automotive, electronics, medical tools, space shuttle, and ballistic amour [1]. Among these, alumina is one of the most cost effective and widely used materials in the family of engineering ceramics since its key properties include excellent hardness and wear resistance, good dielectric properties, resistance to strong acid and alkali attack at elevated temperatures, high thermal conductivity, great variety of size and shape, high strength and stiffness [2]. However, sintering, which is one of manufacturing processes for ceramic material preparations consumes high energy in terms of pressure and temperature [3-5]. Therefore, an exploring of appropriate materials to substitute ceramic in some applications, one has been focused on highly filled polymer composites.

Thermoset polymers are plastics that have been generated using heat or chemicals to crosslink the molecular chains. Once a thermoset is cured, it cannot be re-heated and reshaped. Thermoset materials are generally stronger than thermoplastic materials due to the formation of 3-D network of chemical bonds, and are also better suited to high temperature applications up to the degradation temperature of the materials [6]. Despite the emergence of several new classes of thermosets, high performance polymers and several other new generation materials that are superior in some respects, phenolic resins retain industrial and commercial interest. Phenolic resins are widely used in various applications because of their several desirable properties, such as good mechanical strength, good electrical insulation, and dimensional stability, resistance against various solvents, fire resistance, and low smoke generation. However, a number of short-comings are also associated with these materials. For example, they are rather brittle, have poor shelf life, acid or base catalysts are often used for the preparation of the resins, which potentially corrode the

processing equipment. They usually release by-products such as water, ammonium compounds, and so forth during curing which sometimes affects the properties of cured resins due to the formation of voids. To overcome these problems, recently, a new type of addition cure phenolic system, polybenzoxazines, has been developed [7-9].

Polybenzoxazine, a novel class of phenolic resins, has a wide range of mechanical and physical properties that can be tailored to various needs. The polymer can be synthesized by ring-opening polymerization of the aromatic oxazines with no by-products released upon curing, no catalysts needed, no solvent elimination, and no need of monomer purification [10]. The property balance of the material renders the polymer with good thermal, chemical, electrical, mechanical, and physical properties including very low A-stage viscosity, near-zero shrinkage, low water absorption, high thermal stability, good fire-resistant characteristics, and fast development of mechanical properties as a function of curing conversion [11]. These properties render polybenzoxazine an ideal polymer for composite fabrication.

As major properties particularly, mechanical properties, are strongly dependent on the amount of the filler or reinforcing agent in the composite, maximum packing of the filler in the matrix is one way to assure the formation of near-perfect mechanical and thermal properties. To achieve high packing density composites, the use of large size particles with multimodal particle size distribution and low aspect ratio with smooth surface texture as a second phase were suggested [12]. This kind of filler is normally found in highly mechanical and thermal ceramics, such as aluminum oxide or alumina. Furthermore, the low viscosity resin generally aids in filler mixing during the molding compound preparation. These hypotheses are based on one important assumption that the adhesion between the filler and the matrix resin is good; otherwise, the third phase, an air gap, may occur and will also have a high contribution to the overall integrity of the composites. Therefore, the choice of resin which possesses low melt viscosity and excellent adhesion with the selected filler is preferred and benzoxazine resin is selected in this work.

In this study, we aim to prepare and characterize properties of highly filled systems of alumina-polybenzoxazine composites. Major physical, mechanical and thermal properties of the highly filled polybenzoxazine will be investigated for an

application that requires outstanding characteristics of the alumina filler using benzoxazine resin as a high performance resin binder.

1.2 Objectives

- To prepare alumina (Al_2O_3)-polybenzoxazine (PBA-a) composites using highly filled systems.
- To determine the maximum packing density of alumina filled polybenzoxazine composites.
- To examine physical, mechanical and thermal properties of the highly filled Al_2O_3-PBA-a composites.

1.3 Scopes of Research

1. Synthesize of benzoxazine resin based bisphenol-A and aniline by solventless synthesis technology.
2. Prepare highly filled Al_2O_3-PBA-a composites by varying alumina contents up to its maximum packing density i.e. 50wt%, 60wt%,…, maximum packing density, using alumina powder with average particle size of 5 μm.
3. Evaluate properties of the Al_2O_3-PBA-a composites as follows.
    3.1 Physical properties
        - Interfacial bonding by Scanning Electron Microscope (SEM)
        - Water absorption (ASTM D 570)
        - Density by water replacement technique (ASTM D 792-91)
    3.2 Mechanical properties
        - Dynamic mechanical properties (DMA)
        - Flexural properties (Universal Testing Machine)
        - Hardness (Microhardness Tester)
    3.3 Thermal properties
        - Curing behaviors and glass transition temperature (DSC)
        - Degradation behavior, solid content by Thermogravimetric analyzer (TGA)
    3.4 Evaluate ballistic impact properties (NIJ standard level IIA).

1.4 Procedure of the Study

1. Prepare chemicals, apparatus, and equipment for this research such as alumina, bisphenol A, aniline etc.
2. Determine mixing or processing conditions of the alumina and benzoxazine resin.
3. Examine alumina-benzoxazine by varying compositions of alumina at 50wt%, 60wt%,…, maximum packing density.
4. Evaluate physical, mechanical and thermal properties of alumina–polybenzoxazine composites.
5. Summarize the optimum packing of alumina–polybenzoxazine composites in terms of physical, mechanical and thermal properties which are recommended for application require.
6. Evaluate ballistic impact properties using NIJ standard (Level IIA).

CHAPTER II

THEORY

2.1 Highly Filled Particulate Composites

Highly filled particulate composite materials have been developed and investigated for different applications in the area of dental and orthopedic medicine, structural plastic materials, paper coatings, automotive products, wood composite, electronic packaging, bipolar-plate, erosion resistance and friction wear etc. [24, 13-22]. On the other hand, the properties of the composite depend on the matrix, reinforcement and the adhesion between the filler and the matrix resin [22, 24]. The reinforcement significantly affect the mechanical and thermal properties of particulate composite materials i.e. strength, hardness, wear resistance, heat dissipation, and dimensional stability etc. [25, 26]. Moreover, to achieve high packing density composites, depending on volume, particle size, particle shape, size distribution and nature of filler. Furthermore, the layer of the matrix resin between the particles must be as thin as possible, to such a degree that its mechanical properties are still high enough for the application. This can be achieved by using a resin which has low melt viscosity. Moreover, the low viscosity resin generally aids in filler mixing during the molding compound preparation [22].

2.2 Particle Packing Modifications

2.2.1 Packing Structures

Particle packing is important in most forming processes. The packing density dictates the die fill, binder content, and shrinkage in sintering. Random packing structures are typical of powder metallurgy processing. For mono-sized spheres, the fractional density is between 0.60 and 0.64 [27]. In the case of the actual density, the value depends on the powder characteristics, namely the size and shape, and factors including the adsorbed moisture. For common P/M powders, the packing density

ranges from 30 to 65% of theoretical value; the lower value is representative of irregular and sponge powders [27].

The figure shows that inter-particle friction depends on particle surface irregularities. The greater the surface roughness or the more irregular the particle shape, the lower the packing density will decrease as the shape departs from equiaxed (spherical). Figure 2.1 gives the fractional packing density for various mono-sized irregular particle shapes. As the particle shapes become more rounded (spherical) the packing density increases. The packing of fibers provides an illustration of a decreasing packing density as the particles have a larger length to diameter ratio L/D. Figure 2.2 plots the fractional packing density versus the length to diameter ratio for fibers. Obviously, packing improves as the particles approach a smooth, equiaxed shape [27].

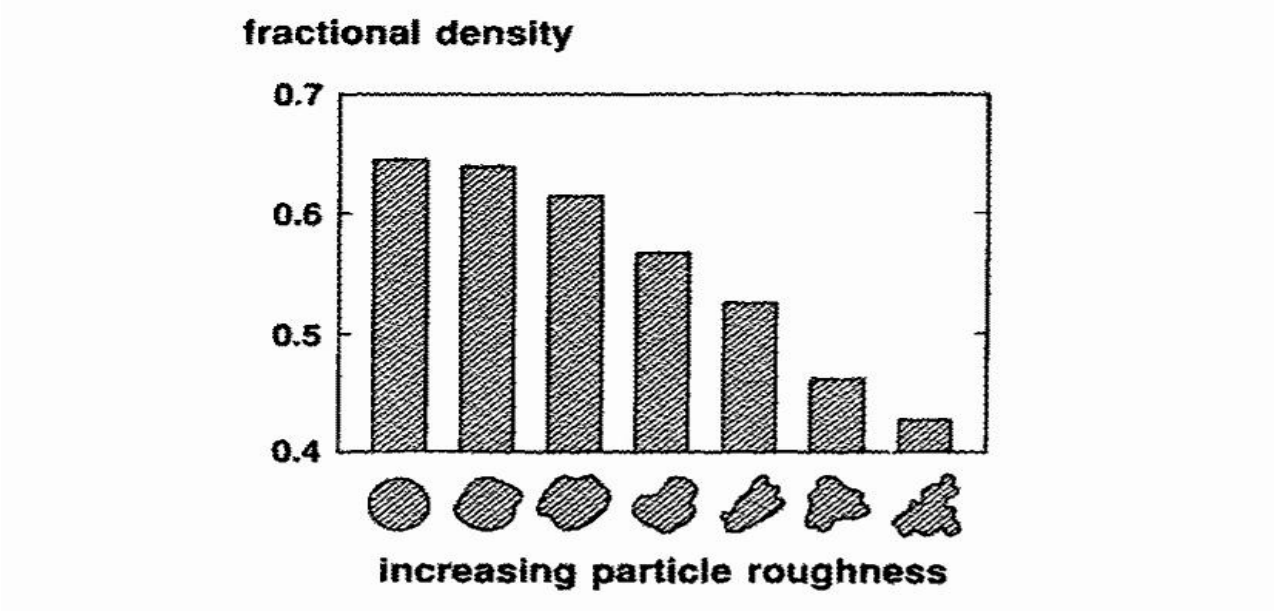

Figure 2.1 Scheme of fraction density for monosized powders versus roughness as expressed by a typical particle profile [27].

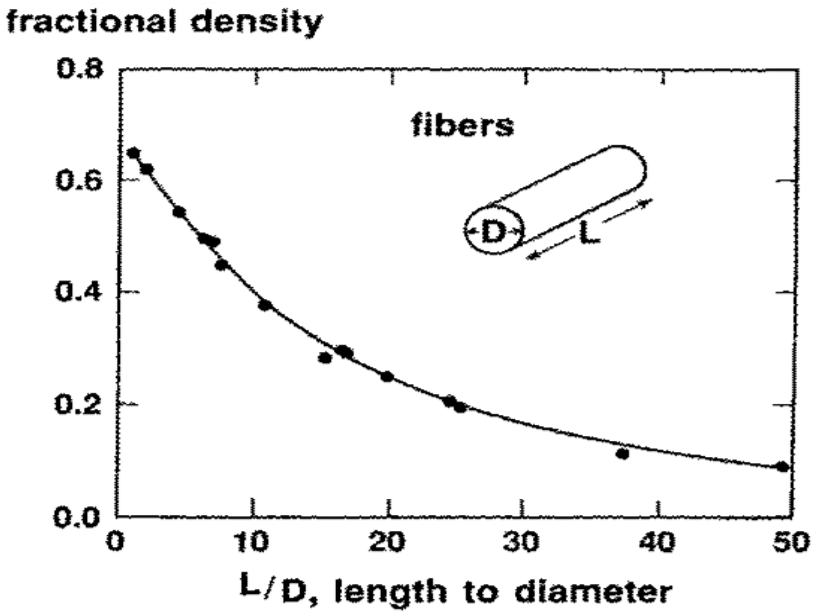

Figure 2.2 Plot of the change in packing density with the length to diameter ratio (L/D) for fibers [27]. (best packing occurs with equiaxed particles.)

2.2.2 Improved Packing Techniques

To overcome the inherent packing limits of a powder, it is possible to tailor the particle size distribution for higher packing density. Bimodal particle blends can pack to higher densities than mono-sized particles. The key to improved packing rests with the particle size ratio. Small particles are selected to fit the interstices between large particles without forcing the large particles apart. In turn, even smaller particles can be select to fit into the remaining pores, giving a corresponding improvement in packing density. The basis behavior is sketched in Figure 2.3. The fraction density is shown as a function of composition for a mixture of large and small spheres. At the maximum packing composition, there is a greater volume of large particles than small particles. The relative improvement in packing density depends on the particle size ratio of the large and small particles. Within a limited range, the greater the size ratio shows the higher the maximum packing density [27].

Beginning with the large particles, the packing density initially increases as small particles are added to fill the voids between the large particles. That corresponds to the right hand side of Figure 2.3. Eventually, the quantity of small particles fills all

of the spaces between the large particles. In contrast, starting with the small particle, clusters of small particles and their associated voids can be removed and replaced with a full density region everywhere a large particle is added. The packing benefit of replacing small particles with the large particle continues until a concentration where the large particles contact one another. Figure 2.3 shows this process as the left-hand plot. The point of maximum packing density corresponds to the intersection of those two curves. At this point, the large particles are in point contact with one another and all of the interstitial voids are filled with the small particles. The optimal composition in terms of the weight fraction of large particle X^* depends on the amount of void spaces between large particles, which equals $1-f_L$, where f_L is the fractional packing density of the large particles,

$$X^* = f_L / f^* \qquad (2.1)$$

with the packing density at the optimal composition f^* given as,

$$f^* = f_L + f_s(1-f_L) \qquad (2.2)$$

and the fraction packing density for the small particle is f_s.

The ideal fraction density of each of spherical powders, i.e., large and small particle sizes, can pack to obtain the maximum packing density is 0.637. To require the maximum packing density value higher than 0.637, the corresponding weight fraction of large particle for maximum packing is 0.734, while the mass fraction of the small particle sizes is of 0.266. The expected fractional packing density would be 0.86 [27].

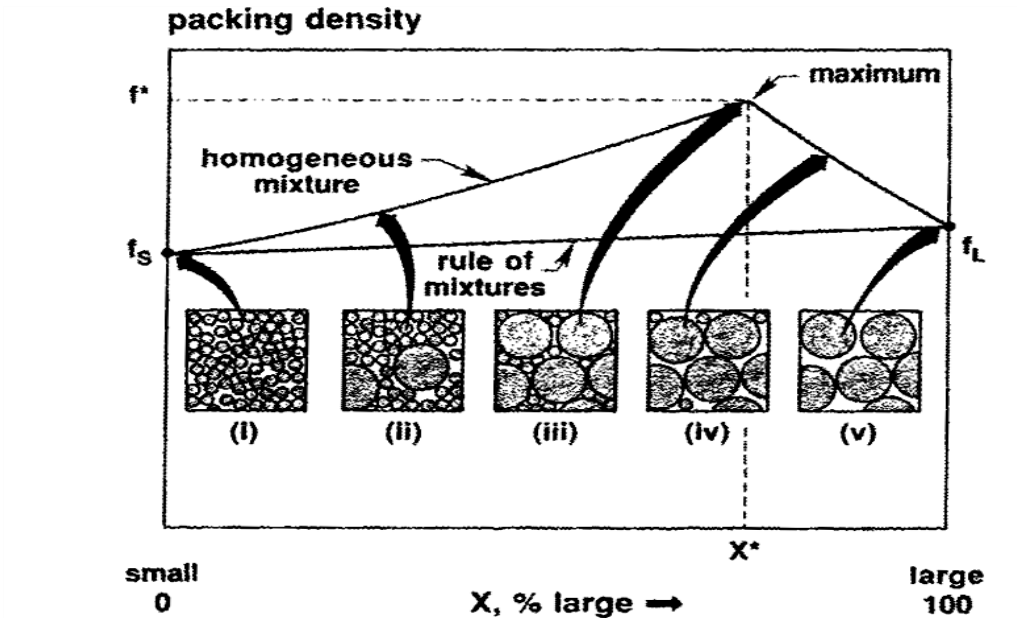

Figure 2.3 Plot of fractional packing density versus composition for bimodal mixtures of large and small spheres [27].

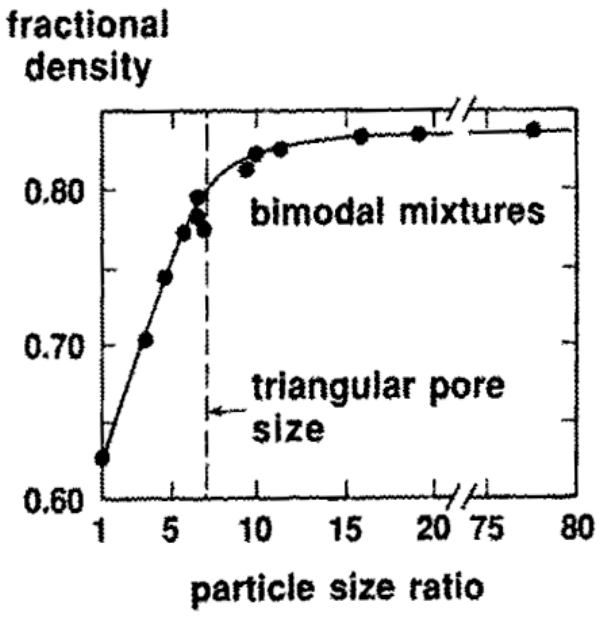

Figure 2.4 Effect of particle size ratio on the packing density for mixtures consisting of 70% large particles and 30% small particles [27].

Figure 2.4 illustrates how the packing density increases with the particle size ratio (large diameter divided by small diameter). Note the dramatic change in behavior at the particle size ratio corresponding to one particle filling the triangular pores between the large particles at roughly a 7:1 size ratio [27].

The packing density will increase with the homogeneity of the mixture. Depending in handling practice, randomly mixed systems will range between unmixed and fully mixed, and typically exhibit some in homogeneities that degrade actual packing from the ideal.

Analogous to the behavior of spheres, a density increase is associated with blending different particle sizes of similar shapes. However, a major difference between spherical and non-spherical particles is that the initial packing is generally higher for spheres. The greater the surface roughness, shape irregularity, or particle aspect ratio, then the lower the inherent packing density. Thus, although the relative density gain is similar for spherical and non-spherical particles, the starting density for non-spherical particles is lower. Accordingly, at all compositions the non-spherical mixture will be lower in density [27].

2.3 Particle Shape

Particle shape is very important in determining the stiffness, or rigidity, of a composite, the flow and rheology of a melt or liquid, tensile and impact strength, and the surface smoothness of composites.

Shape is determined by the genesis of the filler, by its chemistry, its crystal structure and by the processing it has undergone. Unfortunately, typical particles likely to be found in fillers are shown in Figure 2.5 [28]. Another form of inter-particle friction arises from irregularities on the particle surface. The greater the surface roughness or the more irregular the particle shape, then the lower the packing density. Figure 2.6 provides a schematic of the general particle shape and surface roughness effects on the fractional packing density. On the left, the packing density is shown as a function of the relative sphericity, which is defined as the surface area of a

sphere of equivalent volume divided by the actual surface area of the particle. The closer the particle shape is to being spherical, the larger the relative sphericity. On this basis both particle shape and surface texture are included in the relative sphericity. As shown in Figure 2.6, the density improves as the particles approach a spherical shape.

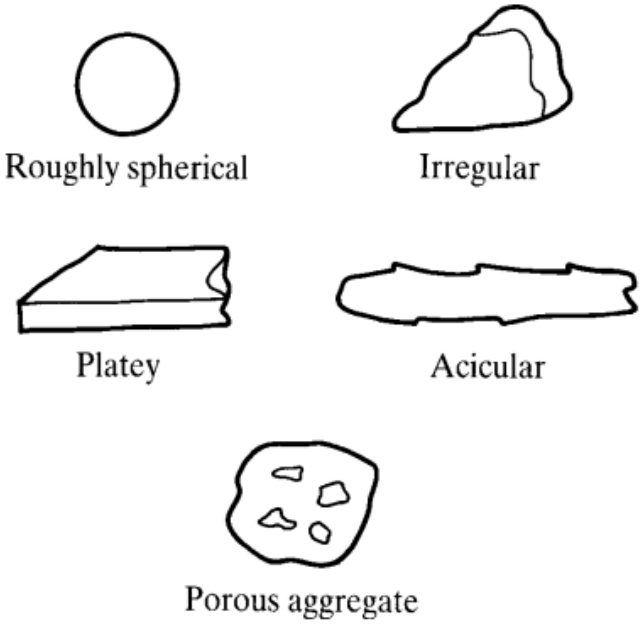

Figure 2.5 Some particle types likely to be found in common fillers [28].

The right half of this figure shows the effect of the relative surface roughness. The relative roughness is a measure of the texture on the powder surface for an otherwise spherical shape. In this regard, the effect of surface roughness is similar to the particle shape effect. This is due to bridging of the particles. The use of vibration or lubricants can help attain a high packing density, but problems may arise with agglomeration or size segregation; however, treatments that increase the surface stickiness of a powder will degrade the packing density [12].

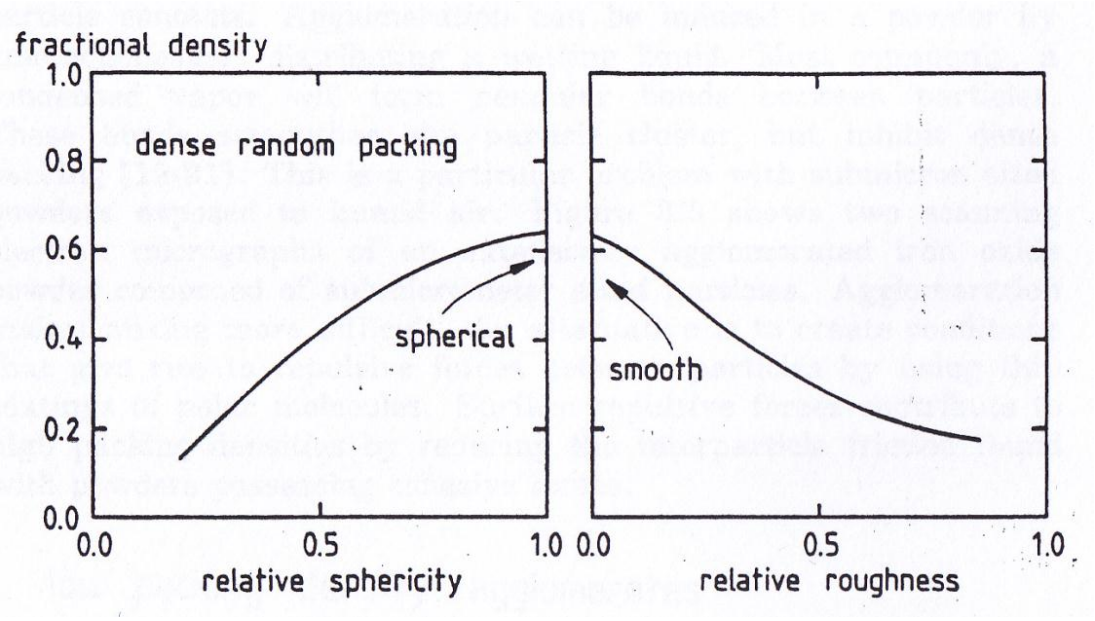

Figure 2.6 Schematic plots of the effect of particle shape and surface texture on the dense random fractional packing density. The highest density is associated with smooth spherical particles [12].

For powders of the same size but different shapes, the packing density will decrease as the shape departs from equiaxed (spherical). This is easily seen in the packing of fibers compared to spheres. The length to diameter ratio provides a measure of the departure from an equiaxed shape. As the shape becomes more fibrous, with a larger ratio of length to diameter, the packing density is reduced. Density can be improved by mixing different sizes of particles. This packing benefit is independent of shape. However, with certain shapes under vibration, a high packing density may be achieved by orienting the irregular particle. Such a high packing density occurs most typically with equiaxed particles. For example, cubic particles can be vibrated to place the cubes in contact along their faces. Such close proximity would give a packing density higher than that attainable with spheres. With a mixture of spherical and irregular powders, the packing density of the spheres is not significantly degraded by the irregular powder until the mixture contains approximately 10% of the irregular power. Thus, the addition of irregular particles

may not harm packing density for spheres, yet may improve compact strength by providing more interparticle friction [12].

2.4 Particle size

Once a stable packing is established, considerable variability is still possible in the structure. For packings composed of large particles, the particles size is not important to the density. However, when the mean particle size is below approximately 100 μm there is more inter-particle friction, and particle bridging is more likely to occur. For example, tungsten carbide particle of 4.6 μm size pack to a 0.55 fractional density, while for those of 1.8 μm size the density is 0.31, and for 0.6 μm size particles the fractional density is 0.12. The decreasing packing density with samller particles is due to an increase in the surface area, a lower paticle mass, and a greater significance of the short-range, weak forces such as electrostatic fields, moisture, and surface adsorption. Since interparticle cohesion increases with a smaller particle size, there is more agglomeration and inhibited packing. As an illustration of this effect, Figure 2.7 shows the packing density for glass spheres as a function of the mean particle diameter on a logarithmic scale. The smaller particles give a lower packing density. The packing densities can be very low for particle sizes significantly below 1 μm [12].

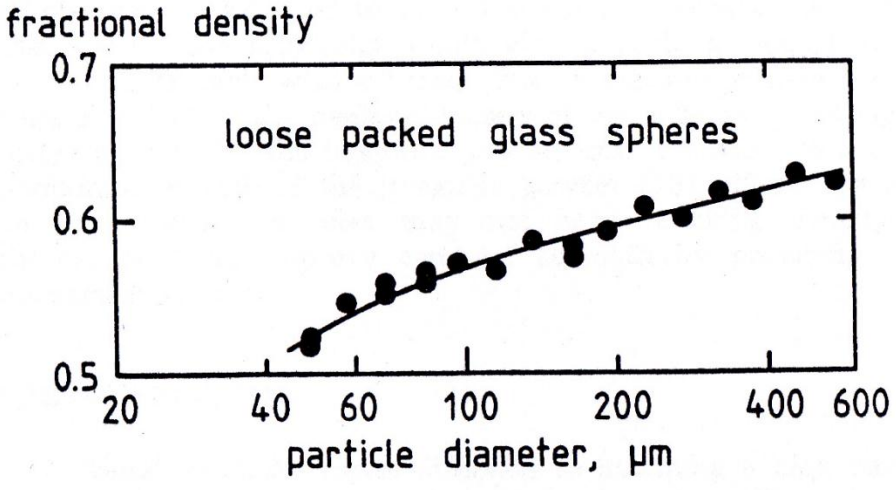

Figure 2.7 A plot of the fractional packing density for loose packed glass spheres versus the particle diameter [12].

2.5 Benzoxazine Resin

Polybenzoxazine is a newly developed class of thermosetting resins. Polybenzoxazine is a phenolic polymer in which generated from phenol, formaldehyde and amine. It can be prepared by using solventless synthesis technology [10]. A novel solventless synthesis method was developed by Ishida in 1996. This method is a convenient method for preparation of benzoxazine monomer series. Stoichiometric amounts of solid bisphenol, para-formaldehyde and liquid 3-aminophenylacetylene were mixed together at 110^{o}C.

Benzoxazine resin can be classified into monofunctional and bifunctional types depending on a type of phenol used as shown in Figure 2.8 and 2.9, respectively.

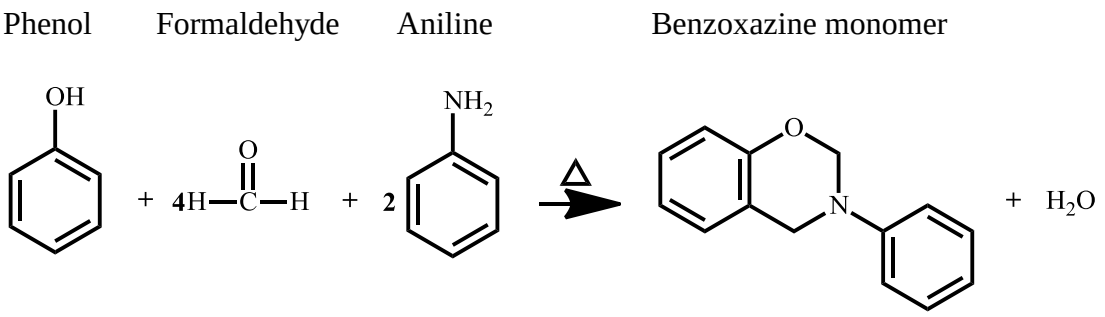

Figure 2.8 Synthesis of monofunctional benzoxazine monomer [10].

Benzoxazine resin can be polymerized by heating and do not need catalyst or curing agent. These two kinds of polybenzoxazine are different in reactant. The benzoxazine monofunction monomer use phenol and the benzoxazine function monomer use bi-phenol to synthesize. Their properties are also different. The bifunctional benzoxazine monomer can be polymerized to yield network structure and was obtained after the polymerization process. The synthesis of benzoxazine resin can be employed by solution or solventless methods.

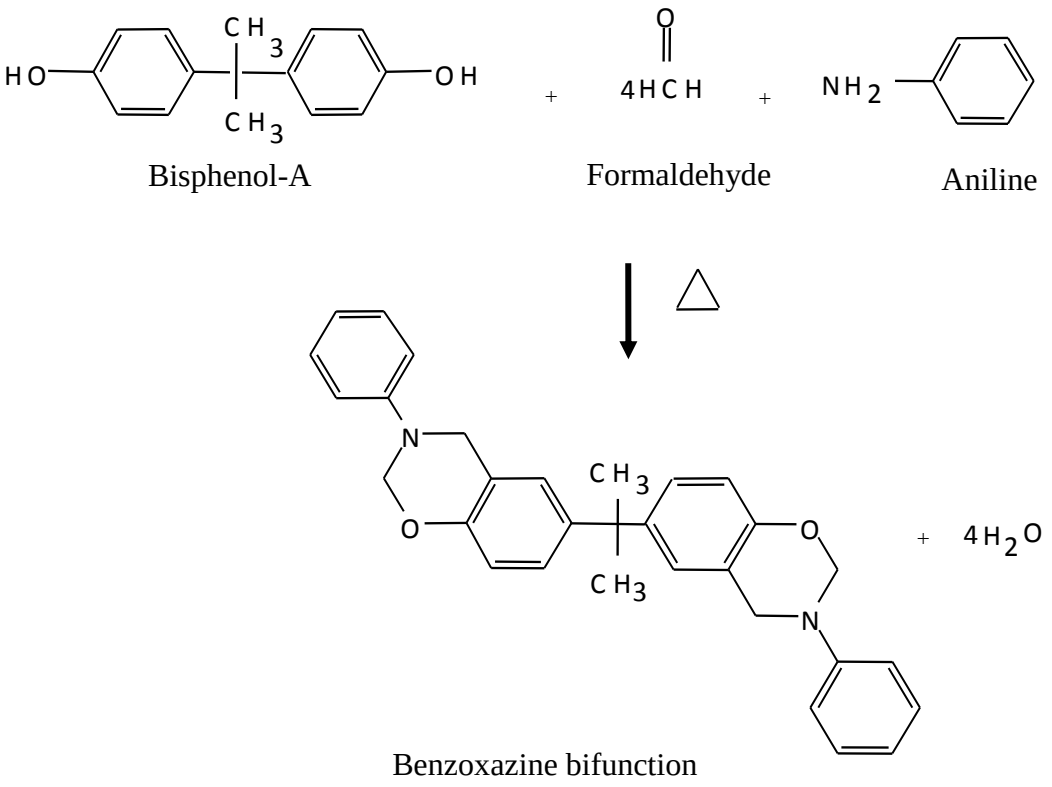

Figure 2.9 Schematic synthesis of bifunctional benzoxazine monomer [10].

The unique properties of benzoxazine resin can be self-polymerized upon heating, catalyst or curing agents required, no by-products during cure, and low melt viscosity. After polymerization, the polybenzoxazine shows outstanding properties such as excellent electrical, thermal and mechanical properties, near-zero volumetric shrinkage upon polymerization and low water absorption.

The other advantages of polybenzoxazine include easy processing ability, lack of volatile formation, all attractive for composite material manufacturing. Furthermore, benzoxazine resin is able to be alloyed with several other polymer or resins. In the literature reported that the mixture of the benzoxazine resin with bisphenol-A typed epoxy [28], which the addition of epoxy to the polybenzoxazine network greatly increases the crosslink density of the thermosetting matrix and strongly influences its mechanical properties.

The properties of polybenzoxazines compared with those of the state of art matrices were depicted in Table 2.1. Polybenzoxazines present the highest

performance; therefore, we use polybenzoxazine resins which will be synthesized from bisphenol-A, formaldehyde and aromatic amine-based (aniline) on this research.

Table 2.1 Comparative properties of various high performance polymers [8].

Property	Epoxy	Phenolics	Toughened BMI	Bisox-phen (40:60)	Cyanate ester	PBA-a
Density (g/cm^3)	1.2-1.25	1.24-1.32	1.2-1.3	1.3	1.1-1.35	1.19
Max use temperature (°C)	180	~200	200	250	150-200	130-280
Tensile strength (MPa)	90-120	24-25	50-90	91	70-130	100-125
Elongation (%)	3-4.3	0.3	3	1.8	0.2-0.4	2.3-2.9
Dielectric constant (1MHz)	3.8-4.5	0.4-10	3.4-3.7	-	2.7-3.0	3-3.5
Cure temperature (°C)	RT-180	150-190	220-300	175-225	180-250	160-220
Cure shrinkage (%)	>3	0.002	0.007	<1	~3	~0
TGA onset (°C)	260-340	300-360	360-400	370-390	400-420	380-400
Tg (°C)	150-220	170	230-380	160-295	250-270	170-340
G_{IC} (J/m^2)	54-100	-	160-250	157-223	-	168
K_{IC} (MPa $m^{1/2}$)	0.6	-	0.85	-	-	0.94

Bismaleimide (BMI), Bisoxazoline-phenolics (Bisox-phen), Polybenzoxazine (PBA-a) Thermogrvimetric analysis (TGA), Fracture energy (G_{IC}), Fracture toughness plain-strain stress intensity factor (K_{IC})

2.6 Alumina

Aluminum oxide, Al_2O_3, commonly referred to as alumina, have found widespread applications, e.g. aerospace, transport, military energy, spark plugs, pumps, missile nose cones, electrical power insulators, abrasives, cutting tools, and electronics packaging. Due to several desirable properties such as high mechanical strength, hardness, thermal stability, excellent corrosion, chemical resistance and wear resistance [2]. Corundum is the most common naturally occurring crystalline form of alumina which alpha alumina is the most stable and most dense. Alpha alumina melts at 2040°C, with creeping and sintering beginning at 1750°C.

Alumina is used in ceramic products in varying amounts. However, discussion is usually limited to high alumina, which refers to those bodies containing 80 percent or more aluminum oxide. The most common alumina is those containing 85, 90, 94, 96, 99, 99.8, and 99.9%. Strength and other properties improve as the alumina percentage increases, but so do cost and complexity of processing. The properties are dependent not only on the alumina content, but also on microstructure and porosity [2].

The 85 percent grade is a general-purpose grade regarded as the workhouse of the industry. It is economical, and provides good wear resistance and strength. Parts fabricated in the 90 percent range provide good wear resistance and strength, and dielectric properties are good for some electrical applications such as interconnection, resistances, and capacitors and is specifically employed in applications such as substrates for hybrid circuits, multi-layer interconnection circuits, materials for type II condensers, and hyper frequency resonators (mobile phones) [30]. The 94 percent alumina is used for multilayer electronic circuits, since it is easily metallized; it sinters at about 1700°C. Grades in excess of 96 percent are usually formed from sub-micrometer powders, which allow them to be fired at lower temperatures. They are characterized by very smooth as-fired surfaces and exhibit high mechanical strength and excellent electrical properties [2].

The thermal and mechanical properties of most of the commercially important high alumina compositions are shown in Table 2.2. The properties of alumina are

significantly affected by composition. In general, these properties improve as alumina content increases. Figure 2.10 shows how thermal conductivity increases as weight percent of alumina increases [2].

In mention above, alumina ceramics are widely used for ballistic protection [31]. Ballistic protection, hardness is most important for this use since the ballistic strength (the shielding effect of a ceramic tile in front of some backing) increases with the hardness [1]. Hardness is the resistance of a mineral to scratching. It is related to the structure of the mineral, the strength of the chemical bonds and the density of packing of its constituent atoms. The mosh scale (Table 2.3), which is still used to rank minerals by their resistance or susceptibility to scratching by other minerals. This scale is widely used for mineral fillers. In this research study, alumina powder will be selected ballistic armor. Specific density of 3.9 g/cm^3 was obtained from the Nippon light metal Co., Ltd.. The size of alumina powder is 5 μm.

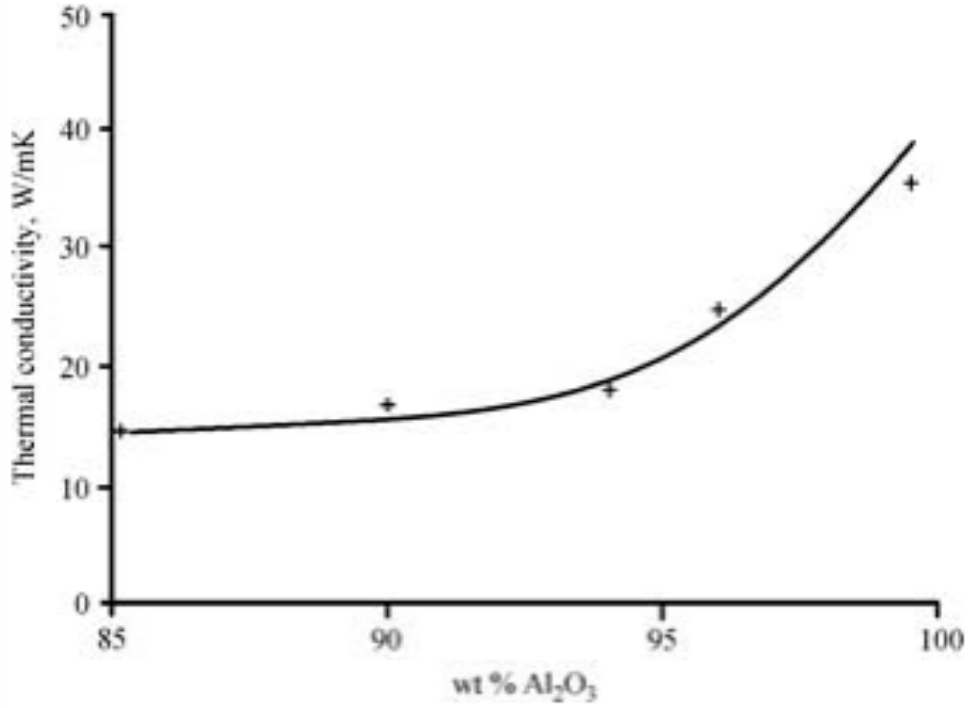

Figure 2.10 Thermal conductivity of alumina compositions increases as alumina content increases [2].

Table 2.2 Thermal and mechanical properties of aluminum oxide ceramics [2].

Property	Aluminum Oxide, weight percent as indicated						
	Units	85	92	94	96	99.5	99.9
Density	g/cm^3	3.41	3.6	3.62	3.72	3.89	3.96
water absorption	%	0	0	0	0	0	0
Coef. Linear thermal expansion	$10^{-6}/K$						
25-200°C		5.3	6.5	6.3	6	7.1	6.5
25-800°C		6.9	7.5	7.6	8	8	7.8
25-1200°C		7.5	-	8.1	8.4	-	8.3
Maximum service temp.	°C	1400	1500	1700	1700	1750	1900
Thermal conductivity	W/cmK						
20°C		0.15	0.16	0.18	0.26	0.36	0.39
100°C		0.12	-	0.14	0.2	0.26	0.28
400°C		0.067	-	0.079	0.12	0.12	0.13
Tensile strength	10^3 lb/in^2						
25°C		22	-	28	38	38	45
1000°C		-	-	15	14	-	32
Compressive strength	10^3 lb/in^2						
25°C		280	-	305	300	380	550
1000°C		-	-	50	-	-	280
Flexural strength	10^3 lb/in^2						
25°C		43	46	51	52	55	80
1000°C		25	-	20	25	-	60
Modulus of elasticity	10^6 lb/ in^2	32	39	41	44	54	56

Table 2.2 Thermal and mechanical properties of aluminum oxide ceramics [2].

Property	Aluminum Oxide, weight percent as indicated						
	Units	85	92	94	96	99.5	99.9
Shear modulus	10^6 lb/in^2	14	-	17	18	22	23
Hardness	R45N	73	-	78	78	83	90
Thermal shock resistance		Moderate			Poor	Excellent	Good

Table 2.3 Mohs scale of mineral hardness [28].

Mohs scale of mineral hardness	**Material**
1	Talc (softest)
2	Gypsum
3	Calcite
4	Fluorite
5	Apatite
6	Orthoclase
7	Quartz
8	Topaz
9	Corundum
10	Diamond (hardest)

CHAPTER III

LITERATURE REVIEWS

H. Ishida and S. Rimdusit, 1998 [10] developed high thermal conductivity obtained by boron nitride-filled polybenzoxazine composites. From the maximizing the formation of highly filled, it was shown that the conductive networks of the large particle size are formed, the thermal conductivity of the composites will exceed that of the smaller particles as the formation of the conductive paths of the large particles renders less thermal resistance along the paths. The phenomenon is more pronounced at the filler content exceeding the maximum packing of smaller particles since the maximum packing of smaller particle size is less than the maximum packing of the larger particles. From Figure 3.1, we have produced a composite with a remarkably high value of thermal conductivity of 32.5 W/mK at 78.5% by volume of boron nitride filler. The value was averaged from the value of 30.8 W/mK at the center of the sample and 34.2 W/mK at the edge of the sample.

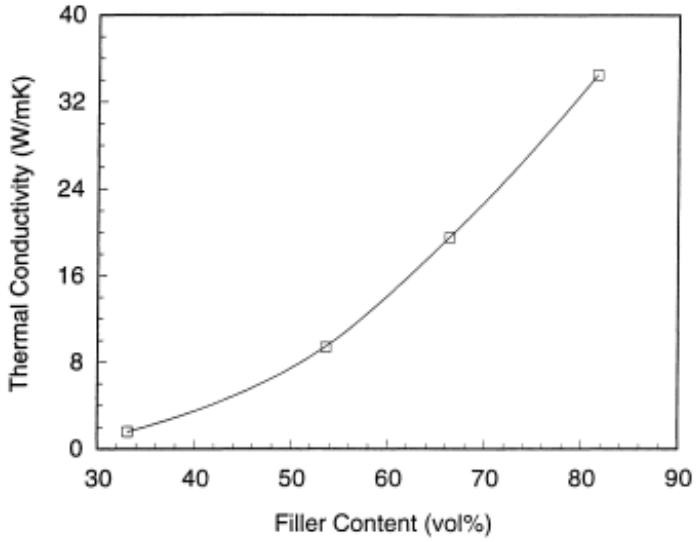

Figure 3.1 Thermal conductivity of boron nitride-filled polybenzoxazine as a function of filler contents [10].

Furthermore, the storage moduli of the composites with filler loadings ranging from 50 to 85% by weight. The moduli of the composites expectedly increase with increasing amount of boron nitride. The modulus at room temperature of 85% by weight filler is very high, exceeding 10 GPa which shown in Figure 3.2. Moreover, the storage modulus of the composite at all compositions exhibited fairly stable values up to ca.200^{o}C due to the high performance properties of the polybenzoxazine matrix. The moduli of these composites increase rapidly and non-linearly with increasing filler contents.

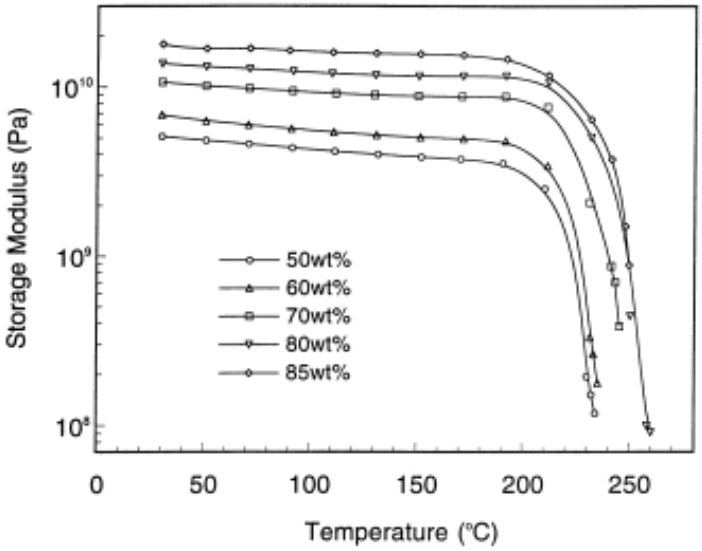

Figure 3.2 Storage modulus of boron nitride-filled polybenzoxazine as a function of temperature at different filler loading. (○) 50 wt.%BN, (Δ) 60 wt.% BN, (□), 70 wt.% BN, (∇) 80 wt.% BN, (◊) 85 wt.% BN [10].

The glass-transition temperatures (T_g) of the filled systems were obtained from the maximum value of G" as shown in Figure 3.3. Increasing tendency of the glass-transition temperature as filler contents increased.

The implication of this phenomenon is possibly due to the contribution of the good interfacial adhesion between the boron nitride filler and polybenzoxazine matrix. The stiff boron nitride filler can highly restrict the mobility of the polymer matrix which adheres on the filler surface and could lead to the large increase in the glass-transition temperatures of their composites.

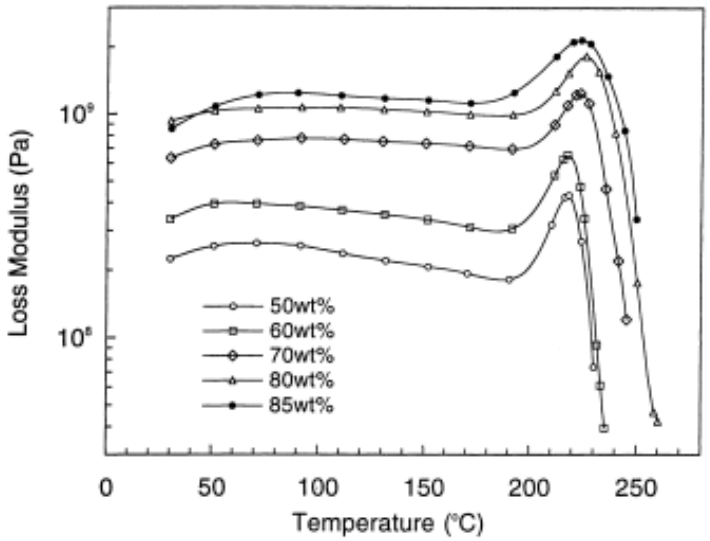

Figure 3.3 Loss modulus of boron nitride-filled polybenzoxazine as a function of temperature at different filler loading. (○) 50 wt.% BN, (□) 60 wt.% BN, (◊) 70 wt.% BN, (Δ) 80 wt.% BN, (●) 85 wt.% BN [10].

S. Rimdusit et al., 2006 [20] developed wood composites from highly filled polybenzoxazine. One measure to determine the optimum packing of the filler in the polybenzoxazine matrix is by composite density measurement. The densities of woodflour-filled polybenzoxazine composites as a function of the woodflour content are shown in Figure 3.4. The results at filler contents in the range of 16.6–70.5% by volume (20–75% by weight) show a linear relationship between the density value and the filler loading. The predicted densities of the neat polybenzoxazine matrix and the woodflour filler were extrapolated to be 1.180 g/cm^3 and 1.442 g/cm^3, respectively. These values are remarkably close to the experimentally obtained densities of the neat resin and the woodflour, i.e., 1.185 g/cm^3 and 1.490 g/cm^3 respectively.

Moreover, the flexural moduli were found to increase with the filler contents from 34.6% by volume to the optimum value at 70.5% by volume, and then slightly decreased at higher filler content due to the insufficient amount of the polymer matrix to wet all the filler particles as shown in Figure 3.5. At a filler content of greater than 70.5% by volume, the load transfer from the matrix to the filler becomes less effective because of the presence of voids

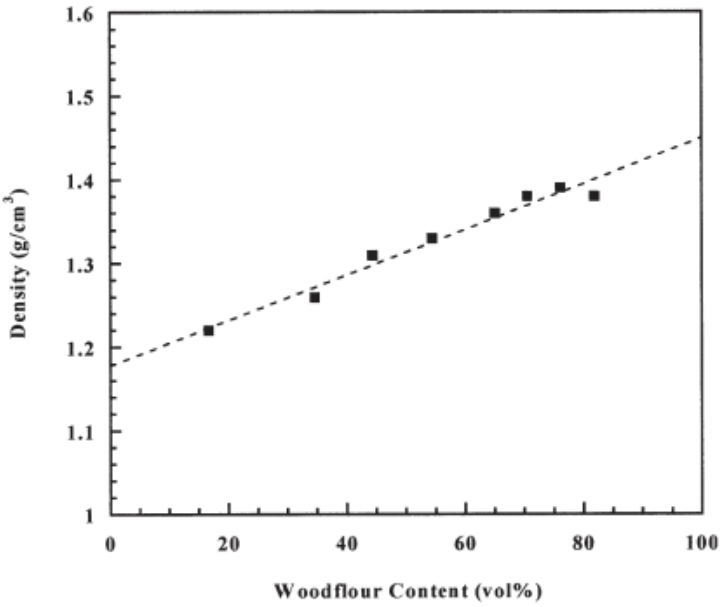

Figure 3.4 The packing density of woodflour-filled polybenzoxazine composite (particle size of Hevea brasiliensis woodflour < 149 μm) [20].

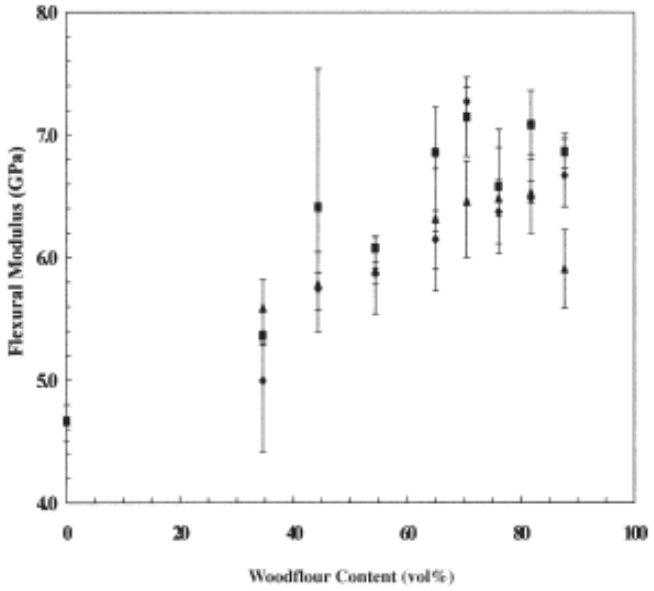

Figure 3.5 Flexural modulus of woodflour-filled polybenzoxazine composites at different filler contents: (■) 420–595 μm, (♦) 250–297 μm, (▲) 149 μm [20].

N. Suprapakorn, et al. 1998 [32] studied the effect of $CaCO_3$ on the mechanical properties of polybenzoxazine. The effects of particle content, particle size, and surface treatment on the flexural strength are shown in Figure. 3.6. Flexural strength decreases with increasing filler content.

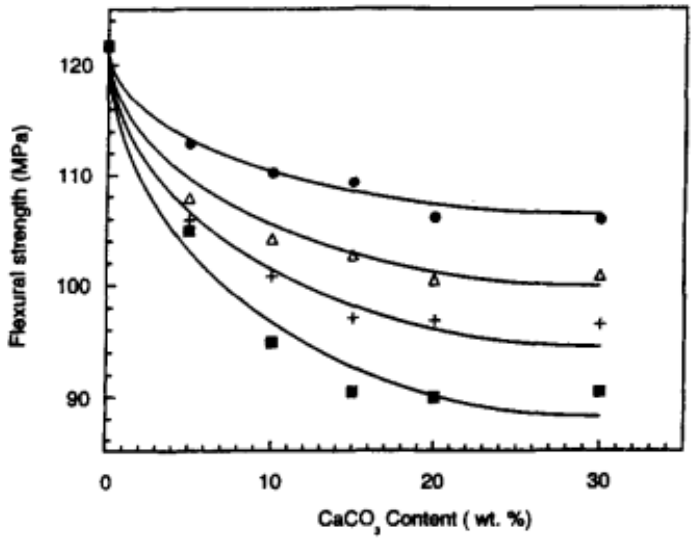

Figure 3.6 Flexural strength of BA-a filled with $CaCO_3$ as a function of the weight percentage, for 5 μm surface treated $CaCO_3$ (■) and untreated $CaCO_3$ with particle size 1 μm (Δ), 5 μm (●), and 20 μm (+) [32].

The composite with surface treated $CaCO_3$, shows lower strength than that of the untreated one. Flexural strength of BA-a/untreated 5 μm $CaCO_3$ is highest among the different particle size. It is possible that the stress at which dewetting occurs depend on the size of the filler. It may be that the untreated 1 μm particles agglomerate to form large particles so that its flexural strength decreases to be lower than that of the untreated 5 μm $CaCO_3$. Moreover, confirm by theoretical predictive models, which are

$$\sigma_c / \sigma_p = (1 - \phi_F^{2/3})S \qquad (3.1)$$

$$\sigma_c / \sigma_p = (1 - K\phi_F^{2/3}) \qquad (3.2)$$

where σ_c and σ_p up are the tensile strength of the composite and matrix, respectively, and ϕ_F is the volume fraction of the filler. The parameter S in Eq. 3.1 accounts for the weakness in the structure caused by the discontinuity in stress

transfer and generation of stress concentration at the filler-polymer interface, as proposed by Nielsen. When there is no stress concentration effect, the S value will be maximum, which equals to unity. The lower the S value, the greater the stress concentration effect. The parameter K in Eq. 3.2 takes into account the adhesion quality between the matrix and the filler. The lower the K value, the better the adhesion.

By using the above equations 3.1 and 3.2, the average values of stress concentration parameter S (Eq. 3.1), and adhesion properties K (Eq. 3.2) in the BA-a/$CaCO_3$ composite can be calculated as in Table 3.1

Table 3.1 The S and K values of BA-a filled with 30 wt% of different types of $CaCO_3$ [32].

Type of $CaCO_3$	**S**	**K**
Surface treated, 5 μm	0.93	1.45
Untreated, 5 μm	0.96	1.28
Untreated, 1 μm	0.74	2.41
Untreated, 20 μm	0.56	3.51

The flexural strength and flexural modulus of the BA-a/ $CaCO_3$, composite are higher than those of polyester/$CaCO_3$ and epoxy/$CaCO_3$, composites, showing that the BA-a/ $CaCO_3$ is much stronger and harder in Table 3.2. It may be because the BA-a structure contains more aromatic rings.

L.M. McGrath, et al. 2008 [33] studied the thermal and mechanical alumina-epoxy composites. The alumina used in the range of 0 – 50 vol% and various particle sizes as shown in Table 3.3.

Table 3.2 The Flexural strength and modulus of $CaCO_3$ filled with BA-a, Polyester, Epoxy [32].

Matrix	**wt% $CaCO_3$**	**Flexural modulus (GPa)**	**Flexural Strength (MPa)**
BA-a	23.1	7.6	106.5
Polyester	23.1	7.1	62
BA-a	28.6	8.0	106
Epoxy	28.6	3.54	31.9

Table 3.3 Al_2O_3 particle size and size distribution [33]

Particle size (μm)	AA2	AA5	AA10	AA18	T60
Mean	3.683	5.064	8.083	16.700	18.81
Mode	3.359	5.064	8.536	18.000	26.14
Standard dev.	1.589	4.878	2.614	4.713	14.45

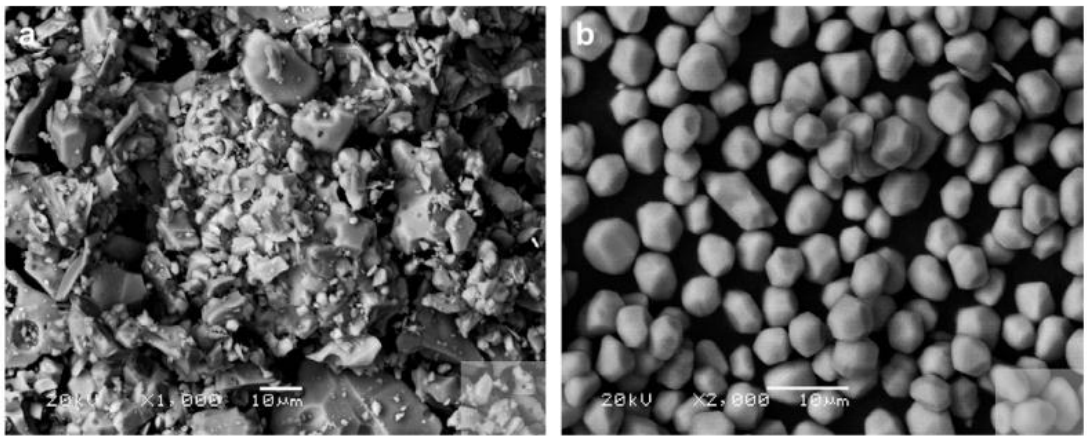

Figure 3.7 SEM micrographs of Al_2O_3: (a) Alcoa T60 and (b) Sumitomo AA5 [33].

the shear storage modulus (G') in the brittle regime (40 ^oC below T_g) and the rubbery regime (40 ^oC above T_g) for the epoxy composites as a function of alumina vol.% loading, filler type, and resin crosslink density as shown in Figure 3.8. We see

that the storage modulus increases with increasing filler content. With increasing particle size (AA5, AA10, AA18, T60), there is no change in either the rubbery or the glassy modulus at each filler loading within experimental.

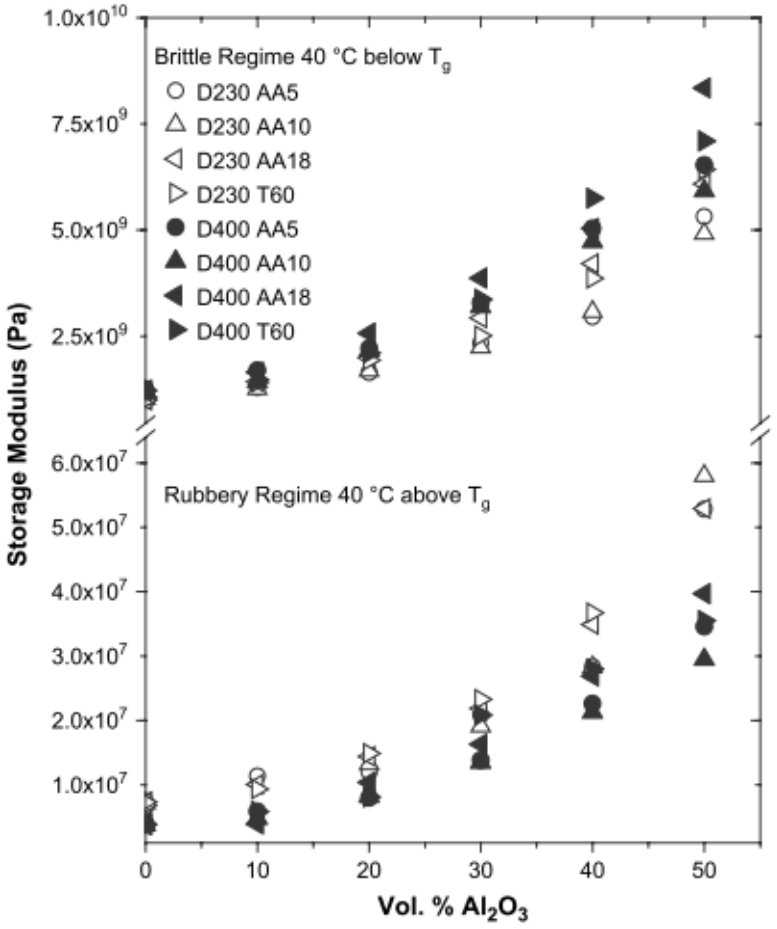

Figure 3.8 (Top) the glassy modulus (T_g – 40 ^oC) for DGEBA/D230 and DGEBA/D400 alumina composites as a function of alumina vol.%; (bottom) the rubbery modulus (T_g + 40 ^oC) for DGEBA/D230 and DGEBA/D400 alumina composites as a function of alumina vol.% and particle type. The error is ± 10% and was determined by multiple sample measurements [33].

This was true for both crosslink density formulations. Comparison of T60 with AA18, which has similar average particle size but different size distribution and shape

(Figure 3.7), indicates that particle size distribution and particle shape have no effect on the glassy or rubbery modulus of these composites.

G' for DGEBA/D230 in the rubbery region is higher than that of DGEBA/D400, at each filler loading, indicative of the higher crosslink density. However, in the brittle region, the storage modulus of the D400 composite systems is slightly greater than that of the D230 system. This trend has shown that the crosslink density, monomer functionality, and chain stiffness have little impact on the glassy modulus.

The coefficient of thermal expansion (CTE) is a critical variable for epoxy composites in electronic packaging. The CTE for the brittle and rubbery regions is shown in Figure 3.9a and b for the DGEBA/D230 and DGEBA/D400 composites, respectively, as a function of filler loading and filler type. The decrease in the rubbery or glassy CTE was independent of the average particle size, size distribution, and shape for both crosslink density systems. This is also consistent with a weak epoxy alumina interfacial region as the thin film polymers research typically shows a decrease in a rubbery CTE with strong polymer substrate interactions. This deviation from rule of mixtures has been observed in filled systems and can be predicted with various types of empirical fitting.

B. Venkatesulu and M. J. Thomas, 2010 [13] studied erosion resistance of alumina-filled silicone rubber. The results at filler contents in the range of 5 – 30 % by weight of microcomposites and 2.5 – 4 % by weight of nanocomposites. Photographs of some of the samples tested using the inclined plane tracking and erosion resistance test apparatus are shown in Figure 3.10 to compare the extent and nature of erosion of the samples. Figure 3.11 and Table 3.4 give the data of the eroded mass, eroded depth, width and length of erosion between the electrodes for the filled and the unfilled composites.

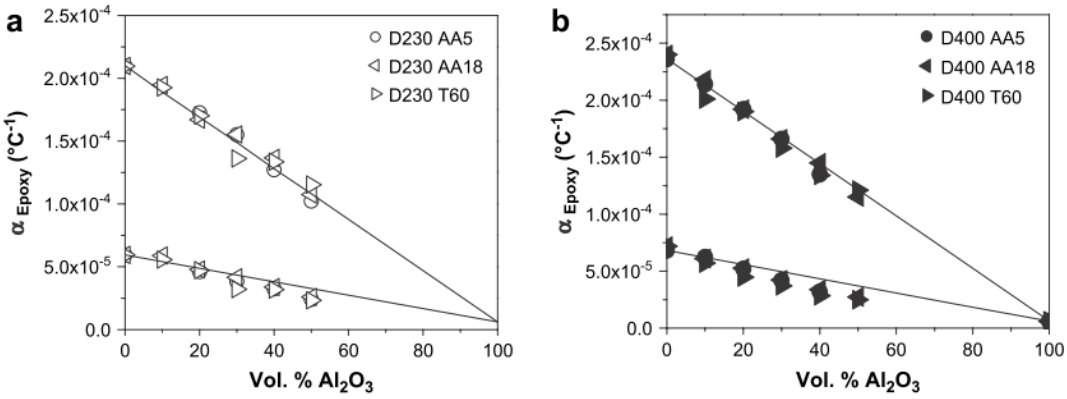

Figure 3.9 The coefficient of thermal expansion as a function of the vol.% of Al_2O_3 in (a) DGEBA/D230 and (b) DGEBA/D400 with various particle sizes (lines represent the theoretical rule of mixtures) [33].

(a) (b) (c)

Figure 3.10 Photographs of Silicone rubber composites of (a) Unfilled, (b) 30% wt ATH (micro) and (c) 4%wt ALU (nano) after 7h of test [13].

Table 3.4 Average values of depth of erosion, eroded width along ground electrode, and eroded length between electrodes for UnF, ATH and ALU composites [13].

Sample	Depth of erosion (mm)	Horizontal width of erosion (mm)	Length of erosion between electrodes (mm)
UnF	4.0	15.2	15.3
5 ATH	4.4	15.8	16.2
10 ATH	3.9	10.8	13.5
15 ATH	4.2	9.9	18.4
20 ATH	3.0	10	5.8
30 ATH	1.8	6.0	3.0
2.5 ALU	2.4	6.6	12.6
4 ALU	2.6	7.0	10.3

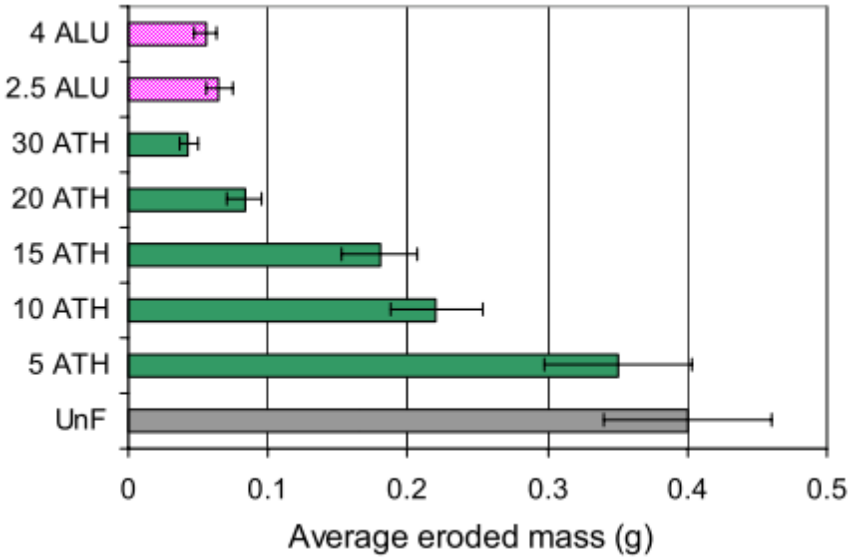

Figure 3.11 Comparison of erosion resistance of different silicone rubber micro and nanocomposites [13].

From the analysis is observed that the performance of unfilled SR is much inferior to filled SR (ATH and ALU) composites. The eroded region of composites as shown in Table 3.4. This width decreases with the increase of filler concentration in the case of ATH. The width of the horizontal eroded track of 30% wt ATH is comparable with the eroded width of 4 ALU. It can be observed in Figure 3.11 that the erosion resistance of the filled composites increases with increase in filler concentrations for both micro and nanocomposites. The spread in the eroded mass is higher at lower filler concentration as the volume occupied by the fillers is less, inter-particle distance is more and the interfacial volume is also less.

CHAPTER IV

EXPERIMENTAL

4.1 Materials and Monomer Preparation

The materials in this research are benzoxazine resin and alumina. Benzoxazine resin (BA-a) is based on bisphenol-A, aniline, and formaldehyde. Thai Polycarbonate Co., Ltd. (TPCC) supplied the bisphenol-A (polycarbonate grade). Paraformaldehyde (AR grade) was purchased from Merck Company and aniline (AR grade) was obtained from Panreac Quimica SA Company. Alumina powder (size: average 4-7 μm) was purchased from purchased from Nippon light metal Co., Ltd.

4.1.1 Benzoxazine Monomer Preparation

The benzoxazine resin used is based on bisphenol-A, aniline and formaldehyde in the molar ratio of 1:4:2. This resin was synthesized by using a patented solventless method in the U.S. Patent 5,543,516. The obtained benzoxazine monomer is clear-yellowish powder at room temperature and can be molten to yield a low viscosity resin at about 70-80 ^{o}C. The product is then ground to fine powder and can be kept in a refrigerator for future-use. The density is 1.2 g/cm^3 and it has a reported dielectric constant of about 3-3.5.

4.1.2 Alumina Characteristics

Al_2O_3 or alumina (SA 31) from Nippon light metal Co., Ltd. The density is 3.9 g/cm^3. It is white powder of α-Crystal. An average diameter of particles of the alumina is ranging from 4 to 7 μm.

4.2 Specimen Preparation

The alumina filled samples were prepared with alumina loadings of 0, 50, 60, 70, 80, and 83% by weight to yield molding compounds. The alumina was firstly dried at 110^{o}C for 24 hours in an air-circulated oven until a constant weight was achieved and was then kept in a desiccator at room temperature. The filler was mechanically stirred to achieve uniform dispersion in benzoxazine resin using an internal mixer at about 110^{o}C. For thermal-cured specimen, the compound was compression-molded by hot pressing. The thickness was controlled by using a metal spacer. The hot-press temperature of 150^{o}C was applied for 1 hour and 200^{o}C for 2 hours using a hydraulic pressure of 15 MPa. All samples were air-cooled to room temperature in the open mold and were cut into desired shapes before testing.

4.3 Characterization Methods

4.3.1 Differential Scanning Calorimetry (DSC)

The curing characteristic of the benzoxazine-graphite composites were examined by using a differential scanning calorimeter (DSC) model 2910 from TA Instrument. For each test, a small amount of the sample ranging from 5-10 mg was placed on the aluminum pan and sealed hermetically with aluminum lids. The experiment was done using a heating rate of 10^{o}C/min to heat the sealed sample from 30^{o}C up 300^{o}C under N_2 purging. The purge nitrogen gas flow rate was maintained to be constant at 50 ml/min. The processing temperature, time and glass transition temperature were obtained from the thermograms while the percentage of resin conversion was calculated from the DSC thermograms.

4.3.2 Density Measurement

Actual Density Measurement

The density of each specimen was determined by water displacement method according to ASTM D 792 (Method A). All specimens were prepared in a rectangular shape (50 mm × 25 mm × 2 mm). Each specimen was weighed in air and in water at 23±2^{o}C. The density was calculated using Equation (4.1). An average value from at least five specimens was calculated.

$$\rho = \frac{A}{A-B} \times \rho_0 \tag{4.1}$$

where ρ = density of the specimen (g/cm^3)

A = weight of the specimen in air (g)

B = weight of the specimen in liquid (water) at 23 ± 2^{o}C (g)

ρ_o = density of the liquid (water) at the given temperature (g/cm^3)

Theoretical Density Measurement

The theoretical density by mass of polybenzoxazine filled with alumina can be calculated as follow:

$$\rho_c = \frac{1}{\frac{W_f}{\rho_f} - \frac{(1-W_f)}{\rho_m}} \tag{4.2}$$

Where ρ_c = composite density, g/cm^3

ρ_f = filler density, g/cm^3

ρ_m = matrix density, g/cm^3

ρ_c = composite density, g/cm^3

W_f = filler weight fraction

$(1-W_f)$ = matrix weight fraction

4.3.3 Dynamic Mechanical Analysis (DMA)

The dynamic mechanical analyzer (DMA) model DMA242 from NETZSCH Instrument was used to investigate dynamic mechanical properties. The dimension of specimens was 50 mm × 10 mm × 2.5 mm (W×L×T). The test was performed under the three-point bending mode. A strain in the range of 0 to 30 μm was applied sinusoidally at a frequency of 1 Hz. The temperature was scanned from 30^{o}C to 300 ^{o}C with a heating rate of 2 ^{o}C /min under nitrogen atmosphere. The glass transition temperature was taken as the maximum point on the loss modulus curve in the temperature sweep tests. The storage modulus (E′), loss modulus (E″), and loss tangent (tanδ) were then obtained. The glass transition temperature (T_g) was taken as the maximum point on the loss modulus curve in the DMA thermogram.

4.3.4 Thermogravimetric Analysis (TGA)

A thermogravimetric analyzer model TGA/SDTA 851^{e} from Mettler-Toledo (Thailand) was used to study thermal stability of alumina: polybenzoxazine composites. The initial mass of the composite to be tested was about 10 mg. It was heated from room temperature to 820^{o}C at a heating rate of 20^{o}C/min under nitrogen atmosphere. The degradation temperature at 5% weight loss and solid residue of each specimen determined at 800^{o}C were recorded for each specimen.

4.3.5 Flexural Properties Measurement

Flexural properties of the polybenzoxazine composite specimens were determined utilizing a Universal Testing Machine (model 5567) from Instron Instrument. The dimension of the specimens is 50 mm × 25 mm × 2 mm. The test method used is a three-point bending mode with a support span of 32 mm. Bending test was performed at the crosshead speed of 0.85 mm/min. The flexural modulus and the flexural strength of each composite were determined according to the procedure set out in ASTM D 790M, they were calculated by Equations 4.5 and Equations 4.6:

$$E_B = \frac{L^3 m}{4bd^3} \tag{4.5}$$

$$S = \frac{3PL}{4bd^2} \tag{4.6}$$

Where E_B = flexural modulus, MPa

S = flexural strength, MPa

P = load at a given point on the load-deflection curve, N

L = support span, mm

b = width of the beam tested, mm

d = depth of the beam tested, mm

m = slope of the tangent to the initial straight-line portion of the load deflection curve, N/mm.

4.3.6 Hardness Measurement

The microhardness of compressed specimens was determined using Vickers hardness tester (Future-Tech Corp FM-700,Tokyo, Japan) at a constant load of 500 gf (4.9 N) and dwell time of 15 s. Diagonal length of the indentation was measured through a micrometric eyepiece with objective lens (50× magnifications). Average values of six readings were reported as the microhardness of the samples.

4.3.7 Water Absorption

Water absorption measurements were conducted following ASTM D570 using disk-shaped specimens having a 50 mm diameter and a 3.0 mm thickness. All specimens were conditioned, weighed, and submerged in distilled water at 25^{o}C. The specimens were occasionally removed, wiped dry, weighed, and immediately returned to the water bath. The amount of water absorbed was calculated based on the initial conditioned mass of each specimen.

4.3.8 Scanning Electron Microscope (SEM)

Interfacial bonding of a filled sample was investigated using an ISM-5400 scanning electron microscope (SEM) at an acceleration voltage of 15 kV. All specimens were coated with thin film of gold using a JEOL ion sputtering device (model JFC-1100E) for 4 min to obtain a thickness of approximately 30Å and the micrographs of the specimen fracture surface were taken. The obtained micrographs were used to qualitatively evaluate the interfacial interaction between the alumina filler and the matrix resin.

4.3.9 Ballistic Impact Test

The ballistic tests were made using one class of ammunitions. The composite panel was tested with a test weapon having an impact velocity following NIJ standard. The velocity of each shot was recorded using a triggered timer system, as shown in Figure 4.1. A test barrel was appropriately selected for the ammunition required to test the armor. The barrel test was mounted in an appropriate fixture with the barrel horizontal. Dimensions A and B shall be determined from the barrel muzzle. The backing material fixture will be rigidly held by a suitable (metal) test stand, which shall permit the entire armor and backing material assembly to be shifted vertically and horizontally such that the entire assembly can be targeted by the test barrel.

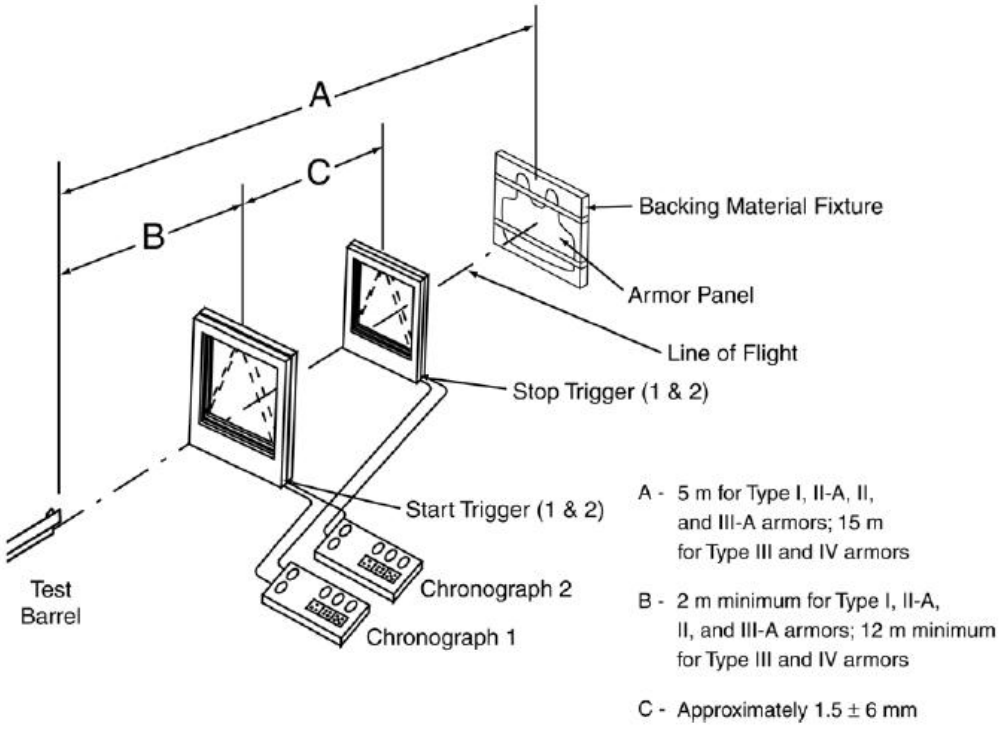

Figure 4.1 Testing scheme used for the NIJ standard ballistic test.

In this research, the ballistic impact test was compared between alumina filled polybenzoxazine composites and glass fiber filled polybenzoxazine composites. The most type of composites will be designed as strike face. The evaluation was performed using a test weapon having impact velocity following NIJ standard. The dimension of the alumina/polybenzoxazine and glass fiber/polybenzoxazine composites were 15 cm×15 cm×1 cm and 15 cm×15 cm×0.3 cm, respectively. The equipment of ballistic test are shown in Figure 4.2

The requirements and acceptance criteria for NIJ standard level II-A are following:

(a) Two complete armor samples, consisting of either a front and back set of armor panels or one full jacket; two samples per test threat.

(b) One fair hit impacts per armor panel or jacket front and back surface for each test threat.

(c) No perforation through the panel, either by the bullet or by any fragment of the bullet or armor.

(a.) Equipments set up following NIJ standard level II-A

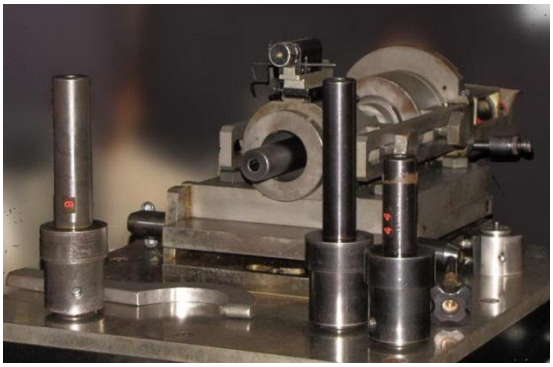

(b.) Test barrel

(c.) 9 mm FMJ RN 124 grains Jacketed Hollow Point

Figure 4.2 The equipment of ballistic test for NIJ standard level II-A.

CHAPTER V

RESULTS AND DISCUSSION

5.1 Alumina-filled Benzoxazine Resin Characterization

5.1.1 Curing Condition Investigation of Benzoxazine Resin Filled with Alumina

Figure 5.1 exhibits the curing exotherms of the neat benzoxazine resin (BA-a) and the benzoxazine-alumina molding compounds at different alumina contents. The thermograms revealed a maximum exothermic peak of all these molding compounds to be at about 231^{o}C, which is the characteristic of this benzoxazine resin [35]. Such exothermic peak reflects the cure characteristic and suggests appropriate thermal curing scheme of the benzoxazine resin. The unchanged exothermic peak position of the benzoxazine molding compounds with an addition of the alumina filler implies that alumina has negligible effect on curing reaction of the benzoxazine monomers e.g. curing retardation or curing acceleration. However, the area under the curing peaks was found to decrease with increasing the alumina content. This expected phenomenon is related to the decreasing amount of benzoxazine resin in the molding compounds with an increase of the alumina content. Curing acceleration of benzoxazine resin had been observed in the mixed systems of cashew nut shell liquid-benzoxazine resin [36], or cardanol-benzoxazine resin [37] while curing retardation was found in epoxy novolac resin-benzoxazine resin [38] etc.

Figure 5.2 presents the DSC thermograms of the benzoxazine molding compound at 50% by weight of the alumina, cured by conventional thermal method. All composites were cured isothermally at 200^{o}C at various times to determine the fully cured stage of the compound. An isothermal cure temperature of 200^{o}C was used in this work because, at this temperature, polymerization by ring-opening reaction of the benzoxazine monomer can proceed at a relatively fast rate and provides good cured specimens. From the experiment, the uncured benzoxazine molding compound

possesses a heat of reaction determined from the area under the exothermic peak to be 201 J/g and the value decreased to 26, 8 and 7 J/g, after curing at 200^{o}C for 1 hour, 2 hours and 3 hours, respectively. The degree of conversion estimated by Equation (5.1) was calculated to be 96% after curing at 200^{o}C for 2 hours and 3 hours, respectively. Therefore, we used a curing time of 2 hours at 200^{o}C and cured every molding compound to provide the final composite samples.

$$\% \text{ conversion} = \left(1 - \frac{H_{rxn}}{H_0}\right) \times 100 \qquad (5.1)$$

Where: H_{rxn} is the heat of reaction of the partially cured specimens.

H_0 is the heat of reaction of the uncured resin.

5.1.2 Actual Density and Theoretical Density Determination of Highly Filled Polybenzoxazine

Figure 5.3 exhibits density of the neat BA-a polybenzoxazine and alumina filled polybenzoxazine composites at 50, 60, 70, 80, 83, and 85wt% of alumina contents. Density measurements of all polybenzoxazine composites were used to effectively examine the presence of void in the composite specimens [22]. This figure also shows the theoretical density of the composites in comparison with their actual or measured density. The theoretical density of the composites was calculated from Equation (4.2) whereas the actual density was calculated by Equation (4.1). The calculation is based on the basis that the densities of the alumina and of the polybenzoxazine are 3.90 g/cm^3 and 1.20 g/cm^3, respectively. The results revealed that the theoretical and actual density of the polybenzoxazine composites was increased with the alumina loading following a rule of mixture. The maximum alumina content up to 60% by volume or 83% by weight was evidently achieved in these highly polybenzoxazine composites. This is because one outstanding property of polybenzoxazine matrix is its low melt viscosity in which the highly filled void-free composite can easily be obtained [20, 22, 23]. However, the attempt to add alumina higher than 60% by volume was found to provide the measured density value to be lower than that of the theoretical value due to the presence of void or air gap in the specimen. Therefore, the maximum alumina loading between the alumina and the polybenzoxazine was found to be about 60% by volume. The maximum filler content

of our BA-a/Al_2O_3 composite is found to be higher than those systems with similar filler particle size or greater particle size such as epoxy/Al_2O_3 composites, epoxy/SCAN (silica-coated aluminum nitride) composites and epoxy/SiO_2 composites etc., as shown in Table 5.1. [39].

5.1.3 Dynamic Mechanical Analysis (DMA) of Highly Filled Polybenzoxazine

Since all polymers are viscoelastic in nature, dynamic mechanical analysis method is suitable to evaluate mechanical properties as a function of temperature as well as complex transition and relaxation phenomena when polymeric materials are presented. Figures 5.4, 5.9 and 5.10 illustrate dynamic mechanical properties of the alumina filled polybenzoxazine composites with the alumina ranging from 0 to 83wt%. At room temperature, the storage modulus (E') of the alumina filled polybenzoxazine steadily increased with increasing alumina content as seen in Figure 5.4. Furthermore, the modulus of the alumina filled polybenzoxazine in the rubbery plateau region was also found to increase significantly with increasing amount of the alumina. This high reinforcing effect from an addition of rigid particulate filler into the polymer matrix is attributed to the strong interfacial interaction between the alumina and the polybenzoxazine.

In general, the modulus of composite material as a function of filler loadings tends to follow a simple rule of mixture. The increase in the modulus value at high alumina loadings in our highly polybenzoxazine composites was observed to be of an exponential type and can be predicted by Lewis and Neilson model as seen in Figure 5.5. The simplest theoretical models to predict the modulus of particle-reinforced polymer composites are the simple rule of mixture (ROM), inverse rule of mixture (I-ROM) and Einstein's equation and can be represent by Equations (5.2), (5.3) and (5.4) respectively. The Einstein equation is valid only at low particle loading when there is perfect adhesion between the particles and the matrix. It is independent of the particle size. It assumes that the particles are much more rigid than that of the matrix [40, 41]. Guth and Smallwood generalized the Einstein concept by introducing a particle interaction term and the modified equation for spherical particle reinforced composites can be represented by Equation (5.5). This equation can thus be applied at

the filler loading higher than Einstein model. Hashin and Shtrikman model can be represented by Equation (5.6). This model is based on macroscopical isotropy and quasi-homogeneous composites, where the shape of the reinforcing particles is not a limiting factor. This model takes into account the Poisson contraction of the particle and matrix where G_m is the shear modulus of matrix.

One of the best models describing the modulus dependence on the filler content for polymer composites is Lewis and Nielsen model, the generalized Kerner equation [42]. Lewis and Nielsen relationship can be represented by Equation (5.7). Where E_c, E_f, E_m are the modulus of the composite, particle, and matrix respectively, V_f, V_m and v_m are the volume fractions of the particle, matrix and Poisson's ratio of the matrix respectively. k_E is Einstein coefficient, which is the value 2.50. A is a constant which depends on the geometry of the filler phase and the Poisson's ratio (v) of the matrix and is defined as Equation 5.8. [42, 43]. In principle, if the particle is not well dispersed and forms agglomerates, the constant A increases [42]. Additionally, B is a constant related to the flexural modulus ratio of the filler particles and the matrix material and given by Equation 5.9. The factor Ψ depends on the maximum packing fraction (Φ_{max}) of the filler as shown by Equation 5.10. In addition, MeGee and McCullough proposed a much more complex equation for Ψ. If the modulus of the filler is much greater than that the polymer and when agglomeration exists in the system. We can approximate Ψ by Equation 5.11 [44].

$E_c = E_m V_m + E_f V_f$ ROM (5.2)

$E_c = E_m E_f / (E_m V_f + E_f V_m)$ I-ROM (5.3)

$E_c = E_m (1 + k_E V_f)$ Einstein (5.4)

$E_c = E_m (1 + 2.5 V_f + 14.1 V_f^2)$ Guth and Smallwood (5.5)

$E_c = E_m + \{V_f / [1 / (E_f - E_m) + 3(1 - V_f) / (3E_m + 4G_m)]\}$ Hashin and Shtrikman (5.6)

$E_c/E_m = (1 + ABV_f) / (1 - B\Psi V_f)$ Lewis and Nielsen (5.7)

$$A = (7 - 5\nu_m) / (8 - 10\nu_m) \quad (5.8)$$

$$B = (E_f/E_m - 1) / (E_f/E_m + A) \quad (5.9)$$

$$\Psi = 1 + [(1 - \Phi_{max}) (1 / \Phi_{max})^2 V_f] \quad (5.10)$$

$$\Psi = 1 + \frac{V_m}{\Phi_{max}} [\Phi_{max} V_f) + (1 - \Phi_{max}) V_m] \quad (5.11)$$

All constants for the matrix and fillers used in the model calculations are listed in Table 5.2. Figure 5.5 shows that the storage modulus of the alumina filled polybenzoxazine composites is situated between the upper bound (ROM) and the lower bound (I-ROM) of the rule of mixture. The ROM and I-ROM consider the constituents of the composites under the iso- strain and iso-stress of the applied load, respectively. However, in particle-reinforced polymer composites, the particles might not be completely separated from one another and there may be particle aggregates on micro-level. Thus, the stress or strain will be distributed unevenly between the particles and aggregates as well as the assumption of either uniform strain or stress is an oversimplification [40]. In addition, these models do not consider size and geometry of the particles and assume perfect adhesion between the particles and matrix. Consequently, our experimental modulus lies in between the upper and lower bounds.

Einstein as well as Guth and Smallwood models evidently underestimate the modulus values for the composites, because it is valid only at low loading for spherical particle and the stiffening or reinforcing action of filler is independent of the size of the filler particles. The equation also assumes the filler to be substantially more rigid than the matrix [40, 41]. In reality, our alumina particles are irregular in shape instead of spherical as shown in Figure 5.15 (a).

The lower bound of the Hashin–Shrikman (H–S lower) model is useful for the polymer–matrix composite, where modulus of the matrix is lower than that of reinforcing particle but with their lower modulus ratio. In our case, this assumption also underestimates the modulus of the composites, which may be attributed to the higher modulus ratio of particles to matrix.

Finally, the Lewis and Neilson model with relatively good fit on storage modulus of the polybenzoxazine composites was obtained when used with the reduced concentration term Ψ as defined by equation 5.11. The value of coefficient A = 1.08 was calculated by equation 5.8 using the reported value of $\nu_{Ba\text{-}A}$ = 0.29 [45]. We used three different values of the maximum packing fraction: Φ_{max} = 0.601 (for random loose packing, non-agglomerated), Φ_{max} = 0.632 (for random close packing, non-agglomerated) and Φ_{max} = 0.37 (for random close packing, agglomerated) for the model fitting. The best fit of the Lewis and Neilson model was obtained when the

maximum packing fraction for random loose packing without agglomeration of the particle i.e. Φ_{max} = 0.601 was used. When an agglomeration of particle (Φ_{max} = 0.37) was used, quite strong deviation of the fitting curve from the experimental data was observed as seen in Figure 5.6. Moreover, if the reduced concentration term Ψ defined by equation 5.10 was used in Lewis and Neilson equation, the experimental data, no matter when values for Φ_{max} are i.e.0.632 or 0.601, was not well predicted by the equation. However, the best fit was obtained when Ψ was estimated by equation 5.11.

For the fitting of the modulus results in Figure5.5 based on the value of Φ_{max} = 0.601, the theoretical value of *A*, calculated by equation 5.8 with Poisson's ratio of the polybenzoxazine,$\nu_{Ba\text{-}A}$ = 0.29 was 1.08. However, the best fitting result was obtained when *A* was further adjusted to 1.2. In principle, higher value of the constant *A* is an indication for the agglomerates existence [42]. From the plot, Lewis and Neilson model can correlate well to our modulus results up to the maximum filler loading of 60 vol% of the alumina filler. This model has also been successfully applied to the system of epoxy/alumina nanocomposite [42], silane coupling agent coated TiO_2-epoxy system [46].

Figure 5.7 shows that the storage modulus at rubbery platu of the alumina filled polybenzoxazine composites is exhibited data fits for the ROM, I-ROM, Guth and Smallwood, Lewis and Nielsen and Einstein models. Lewis and Neilson model with relatively reasonable fit on rubbery platu of the polybenzoxazine composites was obtained when used with the reduced concentration term Ψ as defined by equation 5.11. The value of coefficient *A* = 1.08 was calculated by equation 5.8 using the reported value of $\nu_{Ba\text{-}A}$ = 0.29 [45]. We used three different values of the maximum packing fraction: Φ_{max} = 0.601 (for random loose packing, non-agglomerated), Φ_{max} = 0.632 (for random close packing, non-agglomerated) and Φ_{max} = 0.37 (for random close packing, agglomerated) for the model fitting. The great data fit of the Lewis and Neilson model was obtained when the maximum packing fraction is Φ_{max} = 0.37. The experimental data was observed as seen in Figure 5.8. However, the best fitting result was obtained when *A* was further adjusted to 8. In principle, higher value of the constant *A* is an indication for the agglomerates existence [42]. Also, the value of Φ_{max}, corresponding to the agglomeration of the filler particle (Φ_{max} = 0.37), gives the best fit for the alumina content dependence of the modulus at rubbery platu. Both

parameters, A and Φ_{max} have values indicating the presence of agglomerates in the samples at temperatures above the Tg (Tg + 40^{o}C). From the plot, Lewis and Neilson model can correlate well to our modulus results up to the maximum filler loading of 60 vol% of the alumina filler.

Figure 5.9 exhibits loss modulus (E") curves of the alumina filled polybenzoxazine as a function of temperature. The maximum peak temperature in the loss modulus curve was assigned as a glass transition temperature (T_g) of the specimen. The glass transition temperature of the neat polybenzoxazine was determined to be 172°C whereas the glass transition temperature of the highly filled composites was increased systematically with the alumina content up to about 185-188^{o}C. This behavior has also been observed in the system of CNT (carbon nanotube) filled polybenzoxazine composites, polybenzoxazine/clay nanocomposites and alumina filled epoxy composites [47, 48, 42]. An increase of the T_g with an addition of the alumina suggests good interfacial adhesion between the alumina filler and polybenzoxazine matrix resulting in a high restriction of the mobility of the polymer chains thus the higher T_g observed. In addition, Figure 5.10 exhibits α-relaxation peaks of the loss tangent (tanδ) of the alumina filled polybenzoxazine composites. From the figure, it was found that the peak maxima of the loss tangent were systematically shifted to higher temperature in good agreement with the loss modulus peak. Tanδ curves obtained from the ratio of energy loss (E") to storage energy (E') in sinusoidal deformation. The magnitude of tanδ peak reflects the large scale mobility associated with α relaxation, while the width of tanδ relates to the network homogeneity. The peak height of tanδ was found to decrease with increasing mass fraction of alumina. This confirmed the reduction in segmental mobility chain with the presence of the rigid alumina suggesting substantial adhesion between the polybenzoxazine and the adamantine alumina filler. Finally, the width at half height of the tanδ tended to increase when the alumina content increased implying more network heterogeneity of the composite systems.

5.1.4 Thermal Degradation of Highly Filled Alumina/Polybenzoxazine Composites

Degradation temperature (T_d) is one of the key parameters used to determine temperature stability of polymeric materials. Figure 5.11 exhibits TGA thermograms of the neat polybenzoxazine and alumina filled polybenzoxazine composites at various alumina contents in nitrogen atmosphere. It was observed that pure alumina exhibits outstandingly high thermal stability [49]. On the other hand, the polybenzoxazine matrix possesses a degradation temperature at its 5% weight loss of 317^{o}C and the char residue at 800^{o}C of 23%. These values were consistent with the results reported by Rimdusit et al. [50-56]. From the thermograms, the degradation temperature at 5% weight loss of the alumina filled polybenzoxazine composites clearly increased with increasing alumina content as seen in the Figure 5.12. The decomposition temperature at the highest alumina content of 83% by weight in the polybenzoxazine was determined to be about 389^{o}C which is 72^{o}C greater than that of the unfilled polybenzoxazine. This extraordinary enhancement in the thermal properties of the highly filler polybenzoxazine is likely due to the barrier effect of alumina as well as the strong interfacial interaction of the benzoxazine resin to the alumina. The effect of alumina content on the degradation temperature at 5% weight loss of alumina filled polybenzoxazine composites is also summarized in Table 5.3. The degradation temperature tends to increase with increasing the amount of the inert filler in the polymer matrix had been observed in the systems of graphite platelet particles filled epoxy composites [57], silicon dioxide reinforced epoxy composites [58].

The relationship between alumina contents and solid residue of the highly filled polybenzoxazine composites is also reported in Figure 5.12 and the numerical values listed in Table 5.3. Alumina ceramic filler exhibits very high thermal stability thus does not experience any weight loss in the temperature up to 800^{o}C under the TGA investigation [49]. When the temperature was raised to 800^{o}C, only the polybenzoxazine fraction was decomposed thermally and formed char. Therefore, the amounts of solid residue in this case can be approximated to directly correspond to the content of the alumina filler plus char residue of the polybenzoxazine fraction.

The remained solid residue can also be used to quantify the exact amount of the polybenzoxazine in the composite and the calculated amount from their solid residue was also listed in Table 5.3. The calculated amount of the polybenzoxazine was found to be about the same as the amount of the starting benzoxazine resin in the molding compound preparation.

5.1.5 Mechanical Properties of Alumina Filled Polybenzoxazine

The properties of the composite depend on the matrix, reinforcement, and the interface between them. The matrix must transfer the applied load to the reinforcement [25]. Flexural modulus and flexural strength of the neat polybenzoxazine and alumina filled polybenzoxazine composites are illustrated as a function of alumina content in Figures 5.13 and Figures 5.14 respectively. Flexural modulus is the ratio of stress to strain within the elastic limit and these properties are used to indicate the bending stiffness of the material. Flexural rigidity is an important property for substrate material in order to sustain the flexural loading during service [59]. As seen in this Figure 5.13, the flexural modulus values of the composites were found to be substantially improved by the presence of the alumina up to 83% by weight. The flexural modulus of the neat polybenzoxazine was determined to be 5.22 GPa whereas at 50% to 83% by weight of alumina contents, the modulus of the alumina filled polybenzoxazine composites systematically increased from 10.83 to 36.39 GPa. The phenomenon was due to the fact that with substantial interfacial interaction between the filler and the matrix, the addition of more rigid particulate alumina into the polybenzoxazine matrix was able to effectively improve the stiffness of the resulting polymer composites. In this work, the flexural modulus of alumina filled composite at 83wt% was found to be 600% higher than that of the neat polybenzoxazine. As illustrated in Figure 5.13, it was clearly seen that the fitting curve of flexural modulus which was generated by using Lewis and Nielsen model with $\Phi_{max} = 0.601$ and $A = 1.2$ was also consistent with that of the storage modulus of alumina filled polybenzoxazine composites. Furthermore, Figure 5.14 presents the flexural strength values of the alumina filled polybenzoxazine composite was found to decrease with increasing alumina content in ranging from 0 – 23.38 vol% (0 – 50 wt%) and to increases with increasing alumina content in ranging from 23.38 – 60.00

vol% (50 – 83 wt%). The strength of composites increases ranging from 96.61 to 142.42 MPa. It is postulated that for poorly strength, the stress transfer at the particle/polymer interface is inefficient because of low surface area between particle and matrix due to dewetting which is breaking up of aggregates and occurs at lower filler concentrations [41, 44, 60]. When the alumina contents increase, the surface area of alumina becomes larger, the alumina has high activity during of the matrix. Moreover, increasing in alumina contents have high bonding strength due to good strongly interfacial adhesion between the filler and matrix, which is critical for effective stress transfer leading to high composite strength [60]. This behavior of flexural strength has been observed in the systems of wood polymer composites from eastern redcedar particles reinforced with benzoxazine resin/cashew nut shell liquid copolymer [61], calcined petroleum coke particles filled phenolic resin composites [62].

5.1.6 Microhardness of Alumina Filled Polybenzoxazine

Surface hardness is generally investigated as one of the most important factors that are related to the abrasion and wear resistance of composite materials [44]. Abrasion and wear are especially important in such applications as plastic bearings, floor covering materials, and automobile tires. Rigid fillers are much harder than plastics as measured by most tests, so it is not surprising that such fillers increase the hardness of the composite over that of the polymer. Figure 5.15 reveals the Vickers microhardness (HV) values of the neat polybenzoxazine and alumina filled polybenzoxazine composite at different alumina contents. The surface hardness of the alumina composites increased exponentially with increasing alumina content. That is because the addition of alumina to polybenzoxazine was found to enhance the ability of the composites to resist of the polybenzoxazine deformation and might be attributed to higher hardness of alumina (15.67 GPa) [63] compared to polybenzoxazine (0.388 GPa). Moreover, relatively uniform distribution of alumina particles and decrease in inter-particle distance with increasing particle loading in the matrix results in increase of resistance to indentation of polybenzoxazine matrix. This behavior has been observed in the system of copper filled Al-15%Mg2Si composites [64], carbon nanofiber/polycarbonate composites [65]. The HV value of the alumina

filled polybenzoxazine composites with the alumina contents ranging from of 0 to 60% by volume (0-83% by weight) were 388 to 1123 MPa.

Furthermore, the hardness of composite material as a function of filler loadings tends to follow a simple rule of mixture. The increase in the hardness value of alumina filled polybenzoxazine composite systems was observed to be of an exponential type and can be predicted by Halpin-Tsai model as seen in Figure 5.15. The simplest theoretical models to predict the hardness of particle-reinforced polymer composites are the simple rule of mixture (ROM) and can be represent by Equations (5.12). As shown in Figure 5.15, a wide gap exists between the experimental and the microhardness predicted from the ROM. This can be attributed to the surface coating of alumina particle with a film of matrix and hence, preventing direct particle-particle contact. Moreover, due to much lower maximum packing factor of the alumina particle under applied pressure, micro- or nanocomposites could not resist the indent penetration in proportion of alumina content.

Haipin-Tsai model is a semi-empirical relationship that takes into account the aspect ratio of the reinforcing particles [40]. This model has shown good fitting for modulus because it takes into account the aspect ratio of the reinforcing particles [66]. Zamfirova et al. reported that modulus of ultra-high molecular weight polyethylene increased with increasing microhardness. Therefore, Halpin-Tsai equation was applied for microhardness by replacing symbol of modulus with hardness as shown in Equation 5.13

$$H_c = H_f V_f + H_m V_m \qquad \text{ROM} \qquad (5.12)$$

$$H_c = H_m \left[(1 + \xi\eta V_f) / (1 - \eta V_f)\right] \qquad \text{Halpin – Tsai} \qquad (5.13)$$

$$\eta = \left[(H_f/H_m - 1) / (H_f/H_m + \xi)\right]$$

Where H_c, H_f, H_m are the hardness of the composite, particle, and matrix respectively, V_f, and V_m are the volume fractions of the particle and matrix respectively. ξ is an adjustable parameter. The upper bound is obtained when ξ = infinite and lower bound when $\xi = 0$. The values of ξ depend on the geometry and packing of the particles as well as on the direction of the load relative to the orientation of anisotropic particles. For alumina filled polybenzoxazine composites $\xi = 0.4$ fits will data for this system. Nevertheless, the ξ is an adjustable or curve fitting parameter, and hence fits well the data.

In general, the addition of micro- or nanoparticles to polymer matrices significantly increased the mechanical properties, particularly modulus and hardness, of the composites if the particles are strongly bonded to the polymer matrix [66, 67]. In this work, the HV value of alumina filled composite at 83wt% was found to be 189% higher than that of the neat polybenzoxazine. Moreover, the value of alumina filled polybenzoxazine composites had more significant change than that of nano-clay/polyamide 6 composites [67], carbon nanofiber/epoxy composites, nano-silica/epoxy composites coating [68] and calcined petroleum coke/phenolic composites [62].

5.1.7 Water Absorption of Polybenzoxazine and Alumina Filled Polybenzoxazine Composites at Various Alumina Contents

The mechanism of water diffusion of the composites was studied from the amount of water absorption by the specimens. The amount of water absorbed in the composites was calculated by the weight difference between the samples exposed to distilled water and the wetting and drying cycled samples. The water absorption was calculated from Equation (5.14):

In Equation (5.14), W is the weight of the specimen at time t, and W_d is the weight of the dry specimen.

$$\text{Water absorption (\%)} = \frac{W - W_d}{W_d} \times 100 \qquad (5.14)$$

From the water absorption of alumina filled polybenzoxazine composites at different alumina contents are exhibited in Figure. 5.16, it can be seen that the water absorption curves for polybenzoxazine and the alumina filled polybenzoxazine curves are similar behavior, i.e., the specimens absorbed water more rapidly during first stages (0-24 hours). The water adsorption values of all alumina/PBA-a composites at different filler contents ranging from 50 to 83% by weight had been recorded up to 168 hours of the immersion i.e. beyond their saturation points. These polybenzoxazine composites show room temperature water uptake having values much less than 0.25 and 1.5% at 24 and 168 hours, respectively. One of the common problems of epoxy resins is their relatively high water up-take at saturation. This relatively high water absorption is due to the presence of polar groups in these resins. Polybenzoxazines

also contain polar groups, such as phenolic OH and Mannich base, -CH_2NCH_2-, in each chemical repeat unit. However, polybenzoxazine absorb much less water than epoxy resins [69]. The water uptake of all compositions at 24 hours is <0.11 % and only ca. 0.01% at a filler content of 83% by weight. These values were significantly lower than the water absorption values of previous works such as those of nano-alumina filled epoxy nanocomposites [70]. Moreover, the water absorption of all samples was also observed to systematically decrease with increasing alumina content. The phenomenon was attributed to the presence of the more hydrophobic nature of the alumina filler in the polymer composites. Good interfacial adhesion as well as excellent wetting of benzoxazine resin with the alumina might also contribute to the substantial reduction of the water absorption values by the addition of the alumina.

5.1.8 SEM Characterization of Alumina Filled Composites

Figure 5.17(a) to 5.17(d) shows the SEM micrograph of the alumina, the neat polybenzoxazine and the alumina filled polybenzoxazine, respectively. Figure 5.17(a) show the shape of filler, which alumina is irregular shaped. Figure 5.17(b) to 5.17(c) shows the fracture surface of the neat polybenzoxazine and the alumina filled polybenzoxazine respectively. The alumina-polybenzoxazine composites reinforced with 50 wt% and 83 wt%. The fracture surfaces of the neat polybenzoxazine and the alumina filled polybenzoxazine (Figures 5.17(b) to 5.17(d)) reveal a brittle composite behavior. Fracture steps and small curved structures were generated on the neat polybenzoxazine surface in the direction of crack propagation (Figure 5.17(b)).The composite surfaces appear rougher than those of the neat polybenzoxazine and evidence a larger amount of absorbed fracture energy. Hence, the alumina particles may activate additional energy dissipating fracture mechanisms. Figure 5.17(c) and Figure 5.17(d) shows the SEM micrographs of the alumina filled polybenzoxazine composites with filler content of 50 and 83 % by weight, respectively. The alumina filled composite based on benzoxazine resin relatively shows good alumina distribution and substantial interfacial adhesion between the matrix and the alumina. These results might be attributed to the very low viscosity and good flow-ability of the benzoxazine resin at the molding temperature.

5.1.9 Ballistic Impact Tests of Composite Armors

The ballistic impact test, NIJ ballistic impact, the test was performed of the alumina filled polybenzoxazine composites which was compared to glass fiber filled polybenzoxazine composites. The dimension of the alumina filled polybenzoxazine composites was 15×15×1cm^3 and glass fiber filled polybenzoxazine composites was 15×15×0.3cm^3. All of the composites were fired with a 9 mm FMJ RN 124 grains with impact velocity of 332 m/s as following NIJ standard.

A bullet moving with a constant speed towards all composites that is fixed at both its ends will deform the composites which absorb the energy of the bullet. Eventually, the composites will be broken regardless of the magnitude of the bullet speed. Thus the energy difference of the composites before its interaction with the bullet and just before the onset of fracture gives the maximum absorption energy of the composites. In reality, from the moment of impact, the speed of a bullet would begin to decrease as it hits any object and eventually either the bullet would bounce back as the speed became zero or the bullet would penetrate the object if the initial speed is high enough. Thus the initial bullet speed for a bouncing-back process is estimated by equating the maximum absorption energy of the composites as calculated by Equation 5.14.

$$E_{abs} = E_f - E_i = \frac{1}{2} m v_{ini}^2 \qquad (5.14)$$

Where E_f is the energy of the composites just before breakage and E_i is that after the bullet interaction, m is the mass of the bullet and v_{ini} is the initial bullet velocity.

Ballistic performance of ceramic materials depends on a number of properties. They include density and porosity, hardness, fracture toughness, Young's modulus, sonic velocity, mechanical strength, and some others. Any single property does not have a direct correlation with ballistic performance because the fracture mechanism during the actual bullet impact is very complicated [32].

After the projectile hit the alumina composite, fracturing of the composites structure took place. Next, very small composite propagated along the projectile direction. Table 5.4 shows the overall results of their ballistic performance. The results revealed that the absorbed energy of alumina composites was similar to glass

fiber composites. It indicates that the microstructural features affecting physical and ballistic properties strongly influence crack propagation and energy dissipation mechanisms and ultimately ballistic performance.

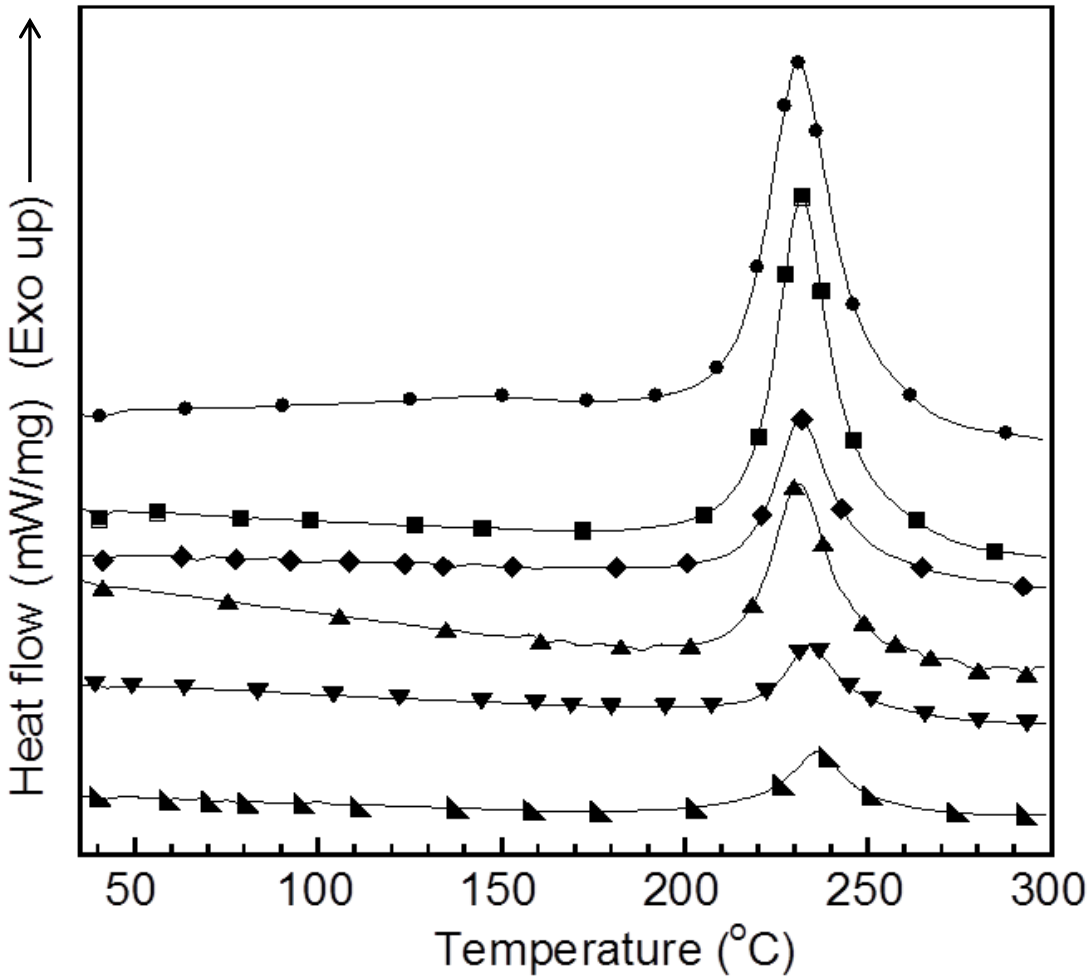

Figure 5.1 DSC thermograms of benzoxazine molding compound at different alumina contents: (●) neat benzoxazine monomer, (■) 50wt%, (♦) 60wt%, (▲) 70wt%, (▼) 80wt%, (◣) 83wt%.

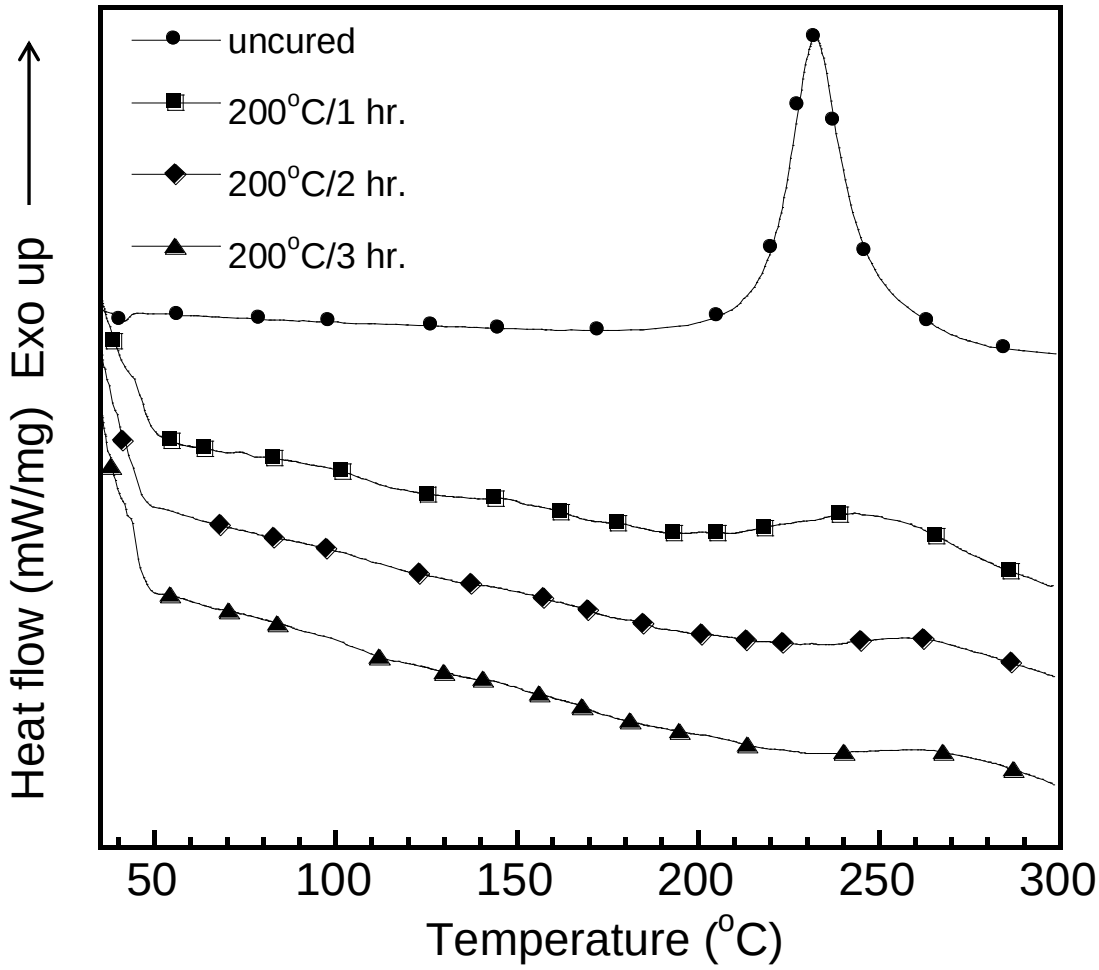

Figure 5.1 DSC thermograms of polybenzoxazine composite (50wt% alumina) at various curing times at 200°C: (●) uncured molding compound, (■) 1 hour, (♦) 2 hours, (▲) 3 hours.

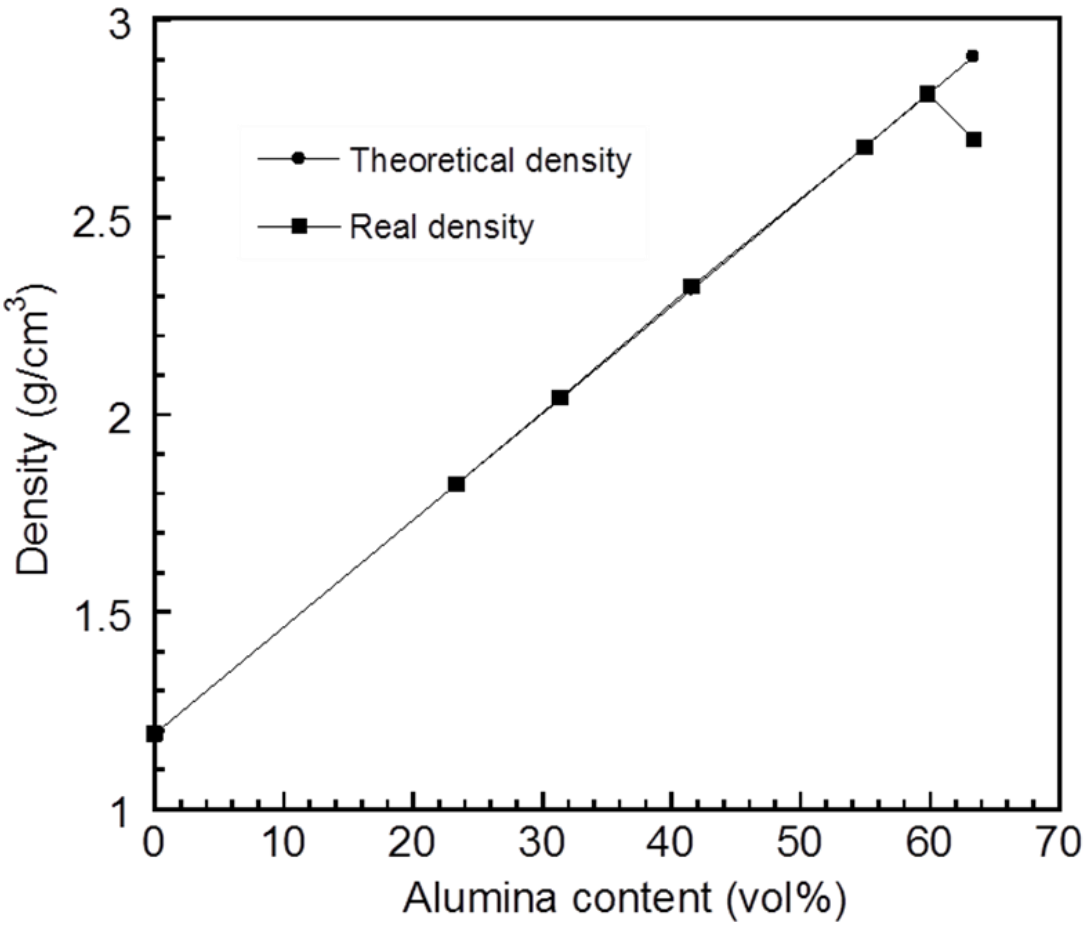

Figure 5.2 Theoretical and actual density of alumina filled polybenzoxazine composites at different contents of alumina: (●) theoretical density, (■) actual density.

Table5.1 Reported maximum alumina contents in various composites and their properties.

Matrix	**Filler**	**Maximum filler content (vol%)**	**Particle size (μm)**	**Young's modulus (GPa)**	**Ref.**
BA-a	Al_2O_3	60	4-7	45.3	
epoxy	Al_2O_3	50	12-15	12	[39]
epoxy	SCAN	50	12-15	15	[39]
epoxy	SiO_2	50	12-15	10	[39]
epoxy	Al_2O_3	50	16.7	7.5	[34]

Table 5.2 Material parameters used in composite modulus predictions.

Parameters	Symbol	Value	Reference
Shear modulus of PBA-a, GPa	G_m	1-3	[45]
Young's modulus of PBA-a, GPa	E_m	5.9	
Young's modulus of Al_2O_3, GPa	E_f	385	[39]
Poisson's ratio of PBA-a	ν_m	0.29	[45]
Poisson's ratio of Al_2O_3,	ν_f	0.24	[39]

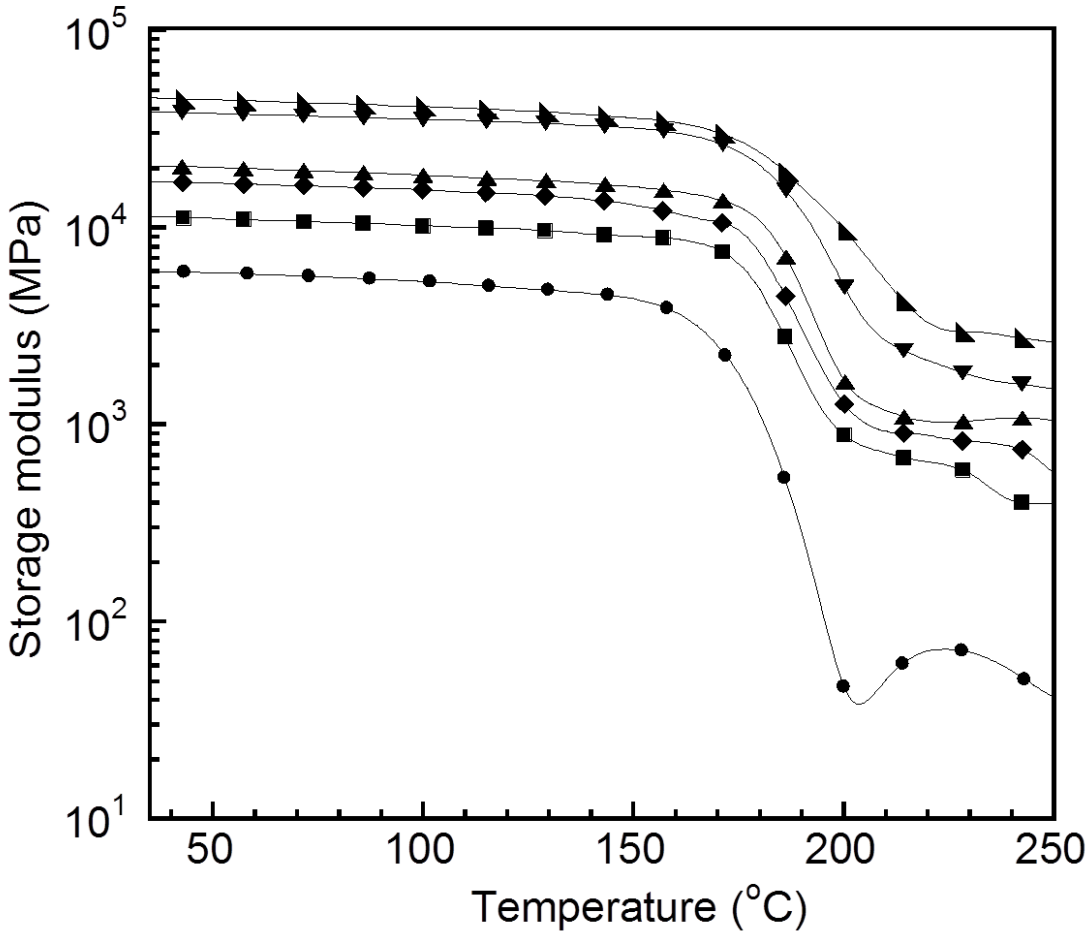

Figure 5.4 Storage modulus of PBA-a/Al_2O_3 composites at various alumina contents: (●) 0wt%, (■) 50wt%, (♦) 60wt%, (▲) 70wt%, (▼)80wt%, (◣) 83wt%.

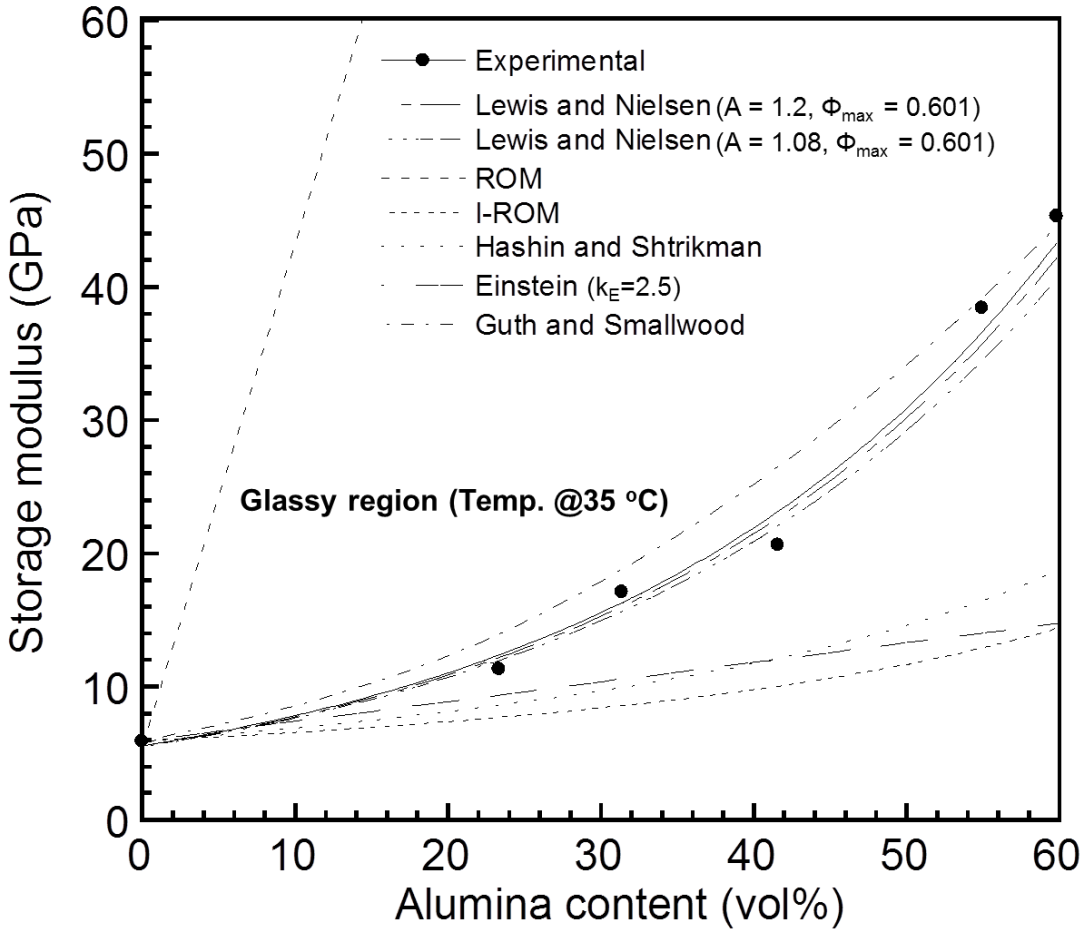

Figure 5.5 Comparison of experimental and theoretical storage modulus of the PBA-a/Al_2O_3 composites at glassy region.

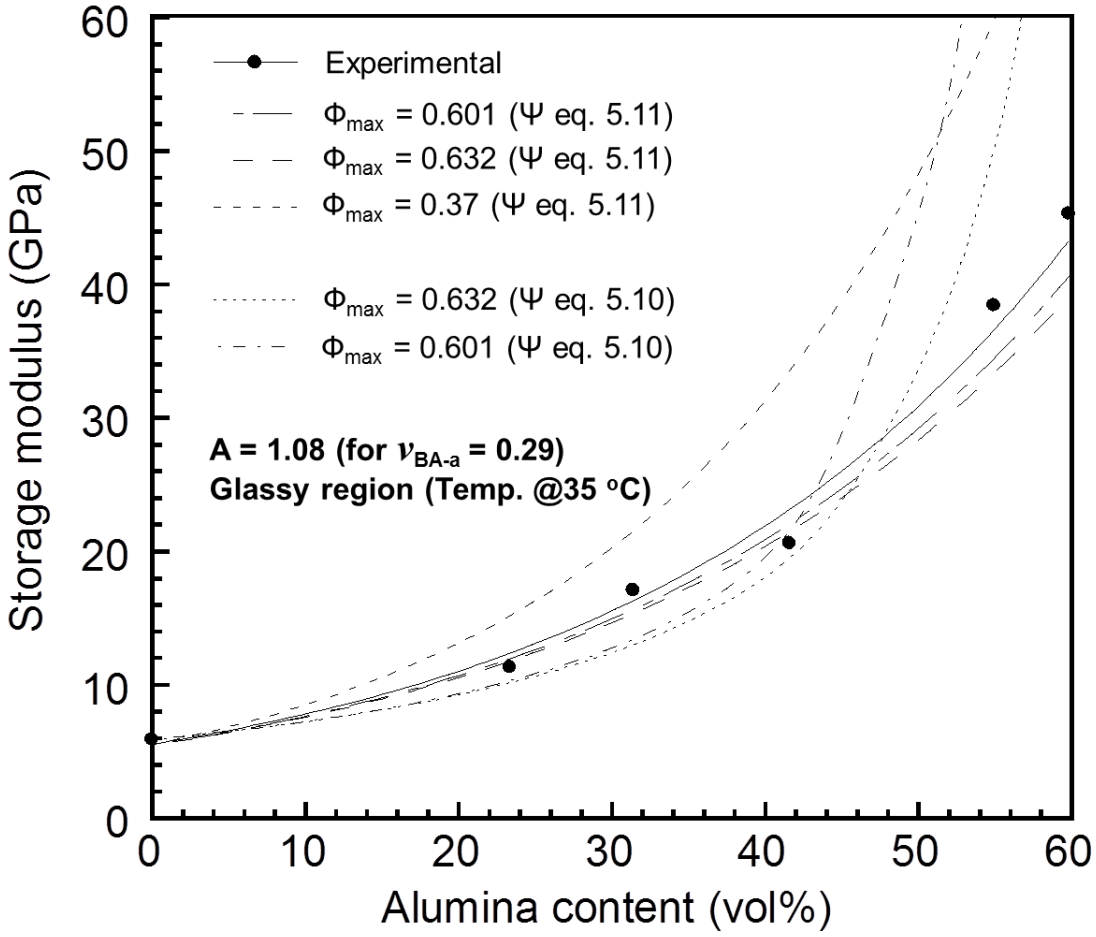

Figure 5.6 Storage modulus at glassy region of PBA-a/Al_2O_3 composites at various maximum packing content from theory.

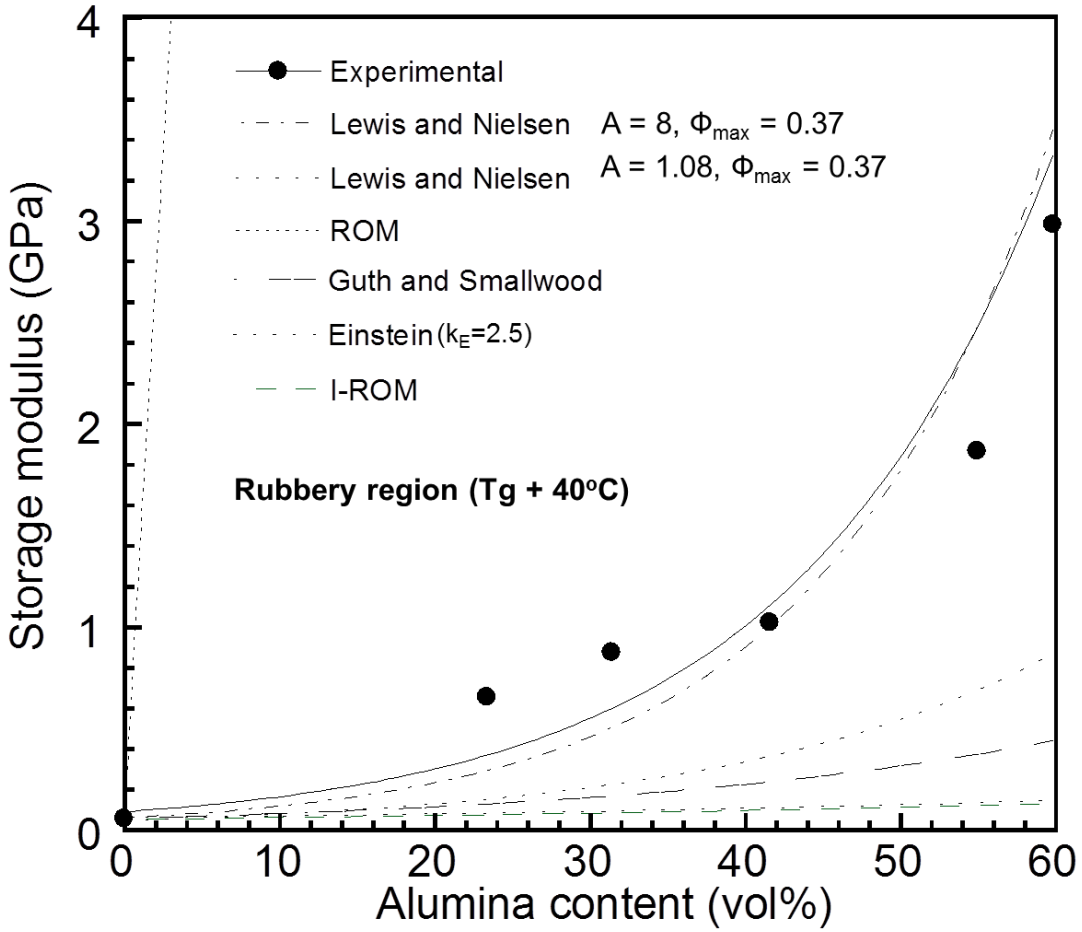

Figure 5.7 Comparison of experimental and theoretical storage modulus of the PBA-a/Al_2O_3 composites at rubbery region.

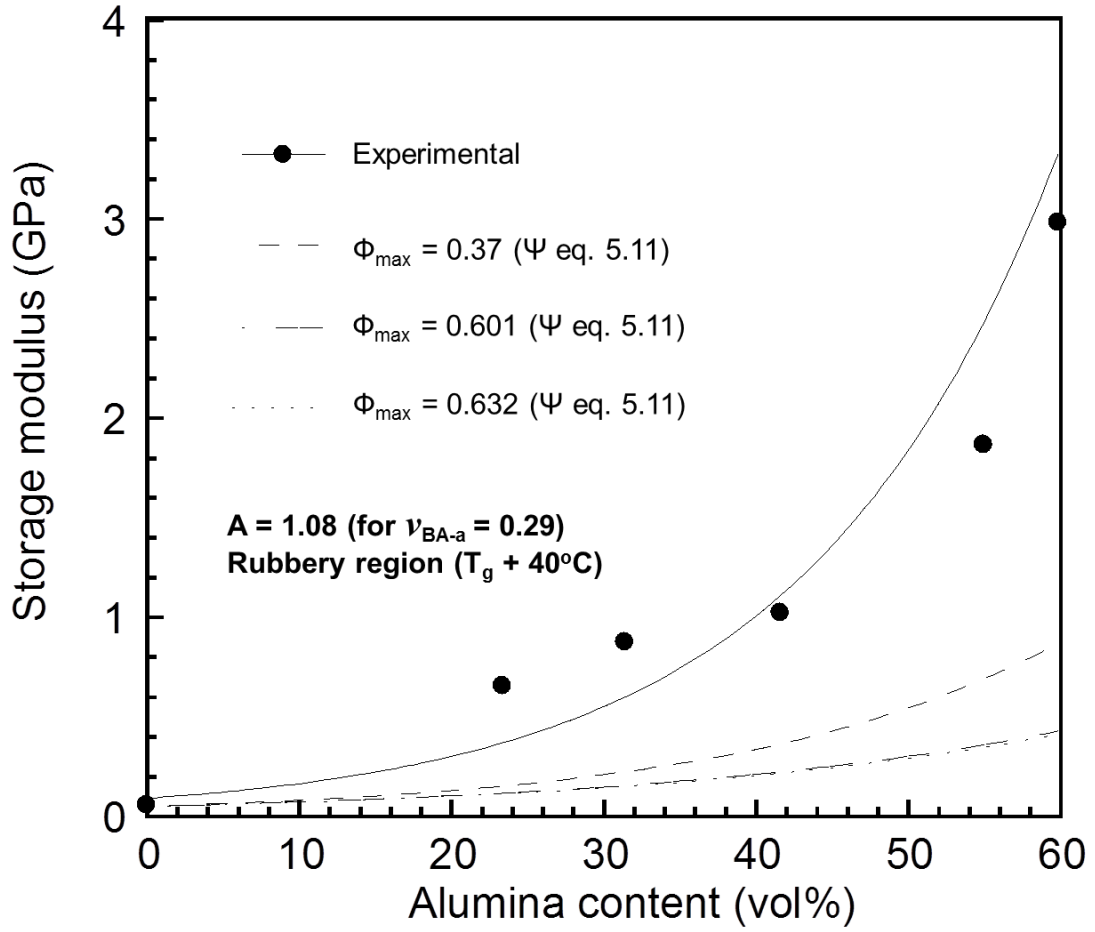

Figure 5.8 Storage modulus at rubbery region of PBA-a/Al_2O_3 composites at various maximum packing content from theory.

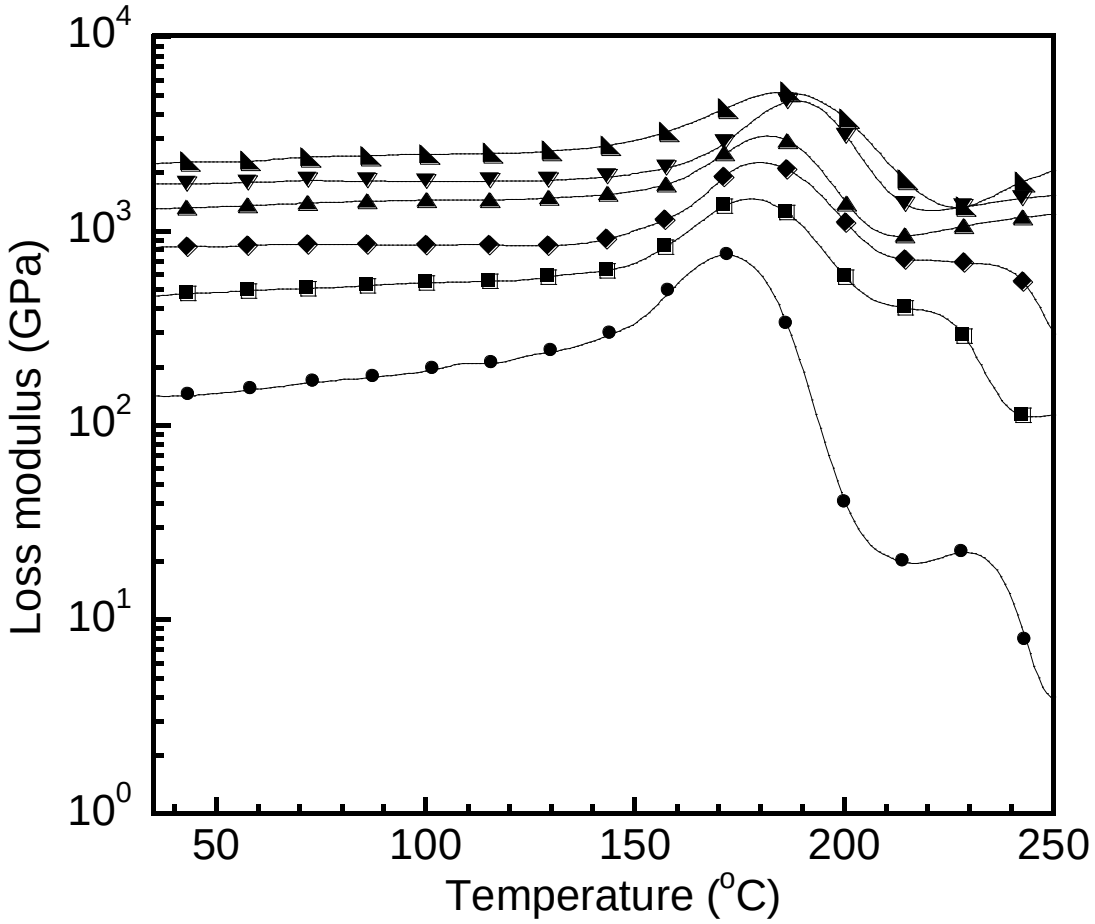

Figure 5.9 Loss modulus of PBA-a/Al_2O_3 composites at various alumina contents: (●) 0wt%, (■) 50wt%, (♦) 60wt%, (▲) 70wt%, (▼) 80wt%, (◣) 83wt%.

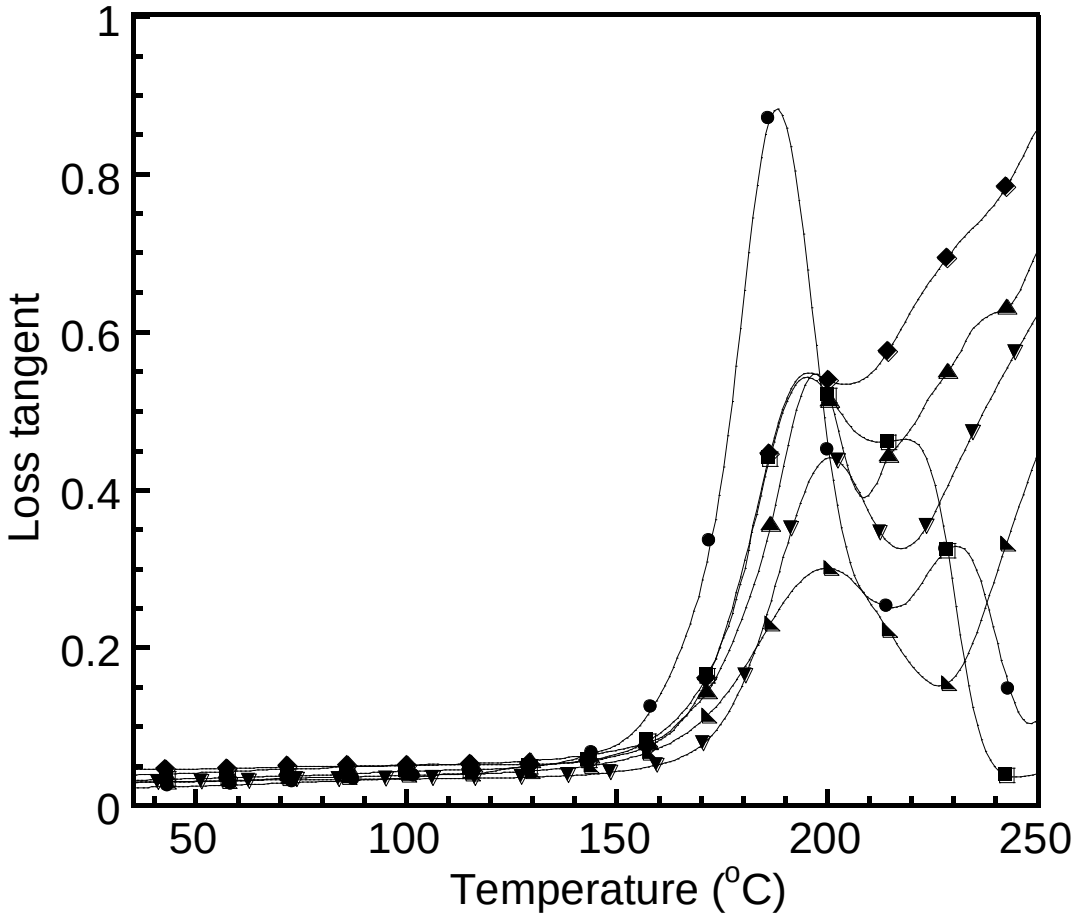

Figure 5.10 Loss tangent of alumina filled polybenzoxazine composites: (●) neat benzoxazine monomer, (■) 50wt%, (♦) 60wt%, (▲) 70wt%, (▼) 80wt%, (◣) 83wt%.

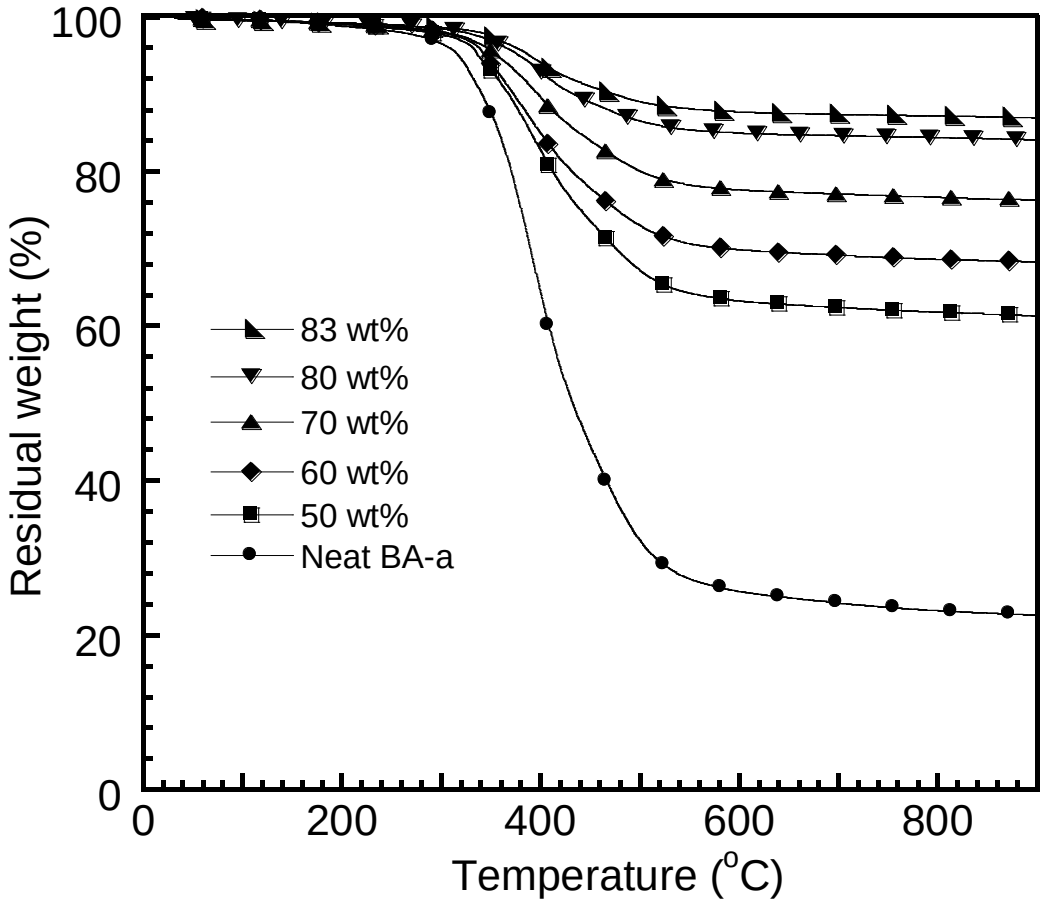

Figure 5.11 TGA thermograms of alumina filled polybenzoxazine composites at various alumina contents: (●) neat polybenzoxazine (■) 50wt%, (♦) 60wt%, (▲) 70wt%, (▼) 80wt%, (◣) 83wt%.

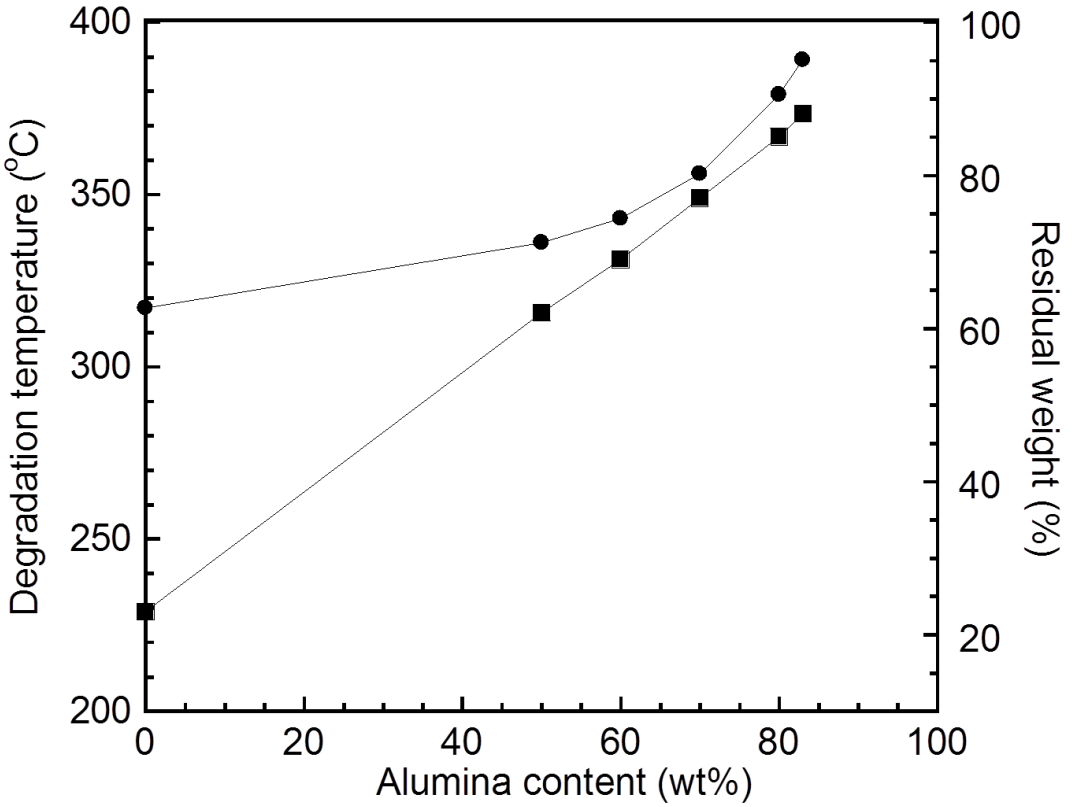

Figure 5.12 (●) Degradation temperature (5% weight loss) of alumina filled polybenzoxazine composites and (■) char yield at 800°C.

Table 5.3 Degradation temperature and residual weight of highly filled Al_2O_3/PBA-a composites.

Alumina content (wt%)	Degradation Temperature (^oC) at 5% weight loss	Solid residue (%) at 800^oC	Exact amount of PBA-a in the composites (wt%)
0	317	23	100
50	336	62	49.4
60	343	69	40.3
70	356	77	30.0
80	379	85	19.5
83	389	88	15.6

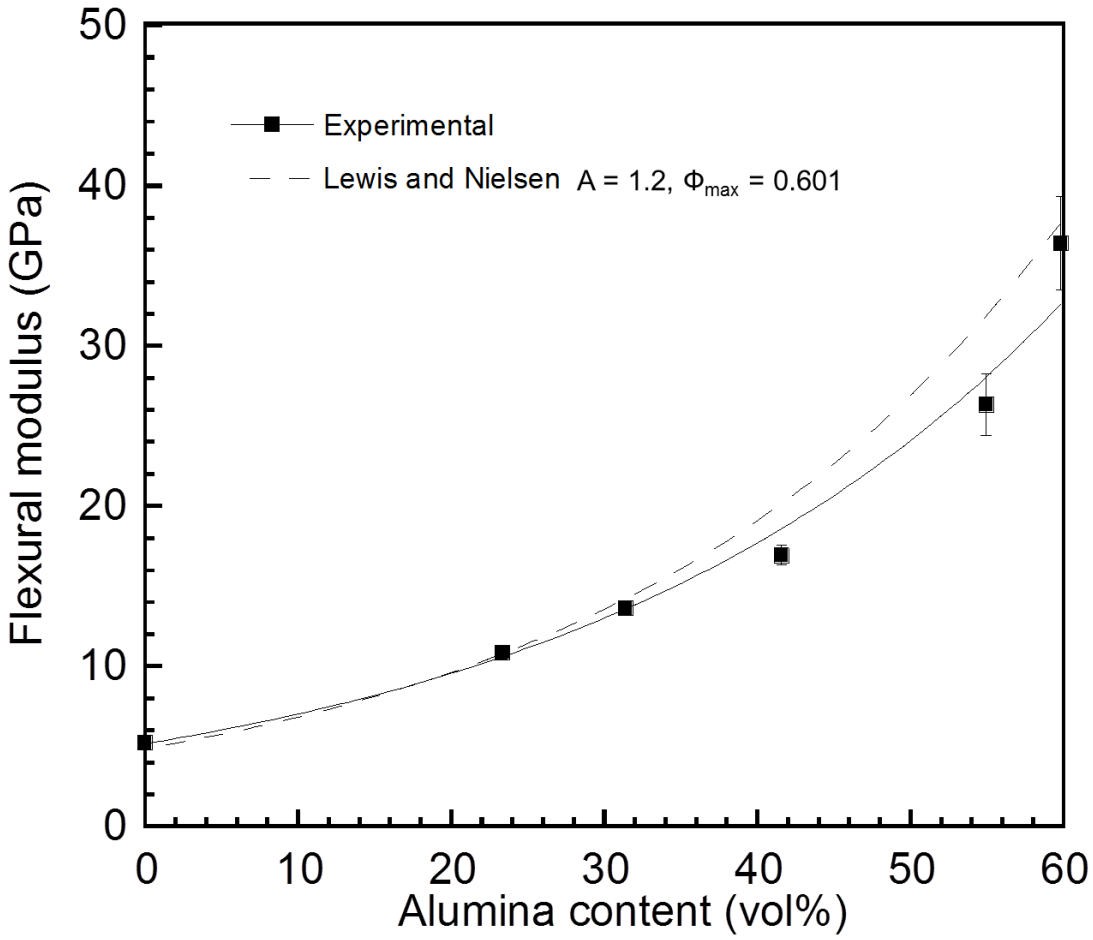

Figure 5.13 Relation between alumina content and the flexural modulus of alumina filled polybenzoxazine composites.

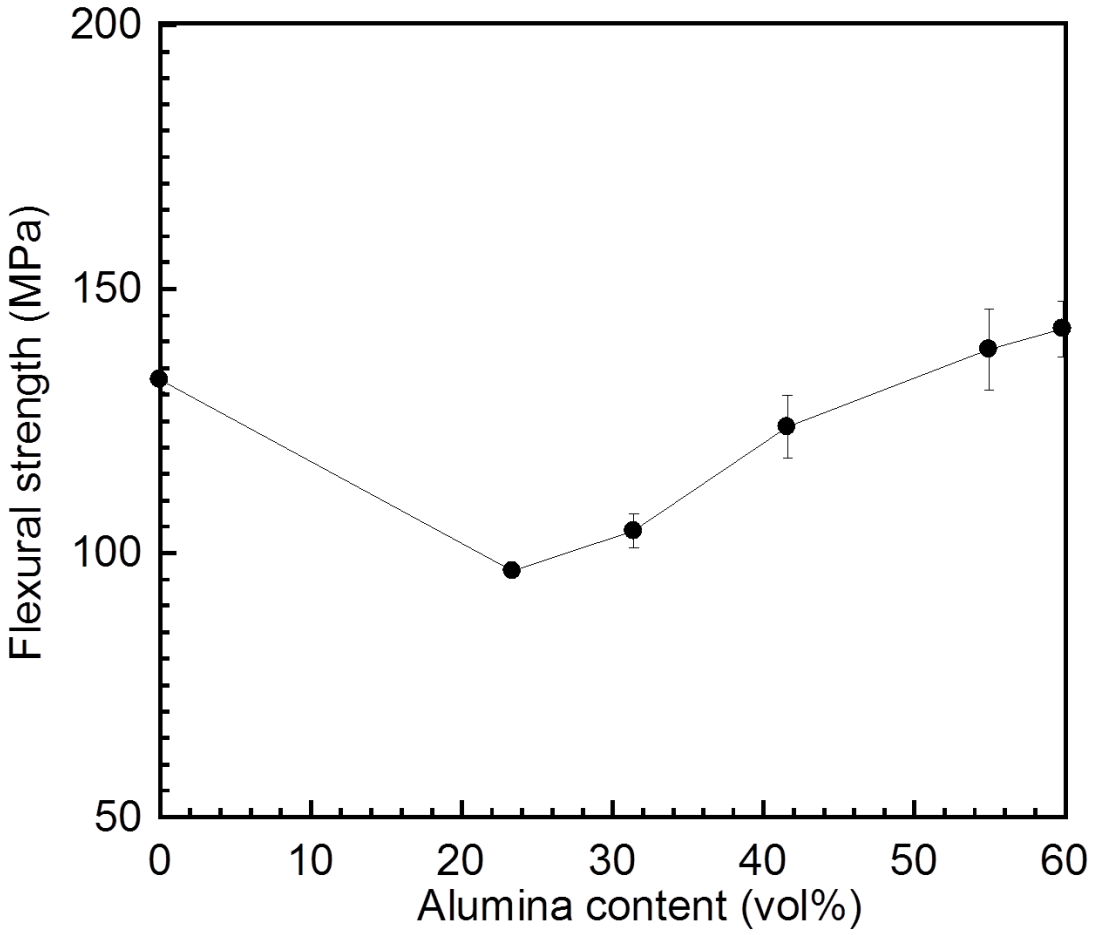

Figure 5.14 Relation between alumina content and the flexural strength of alumina filled polybenzoxazine composites.

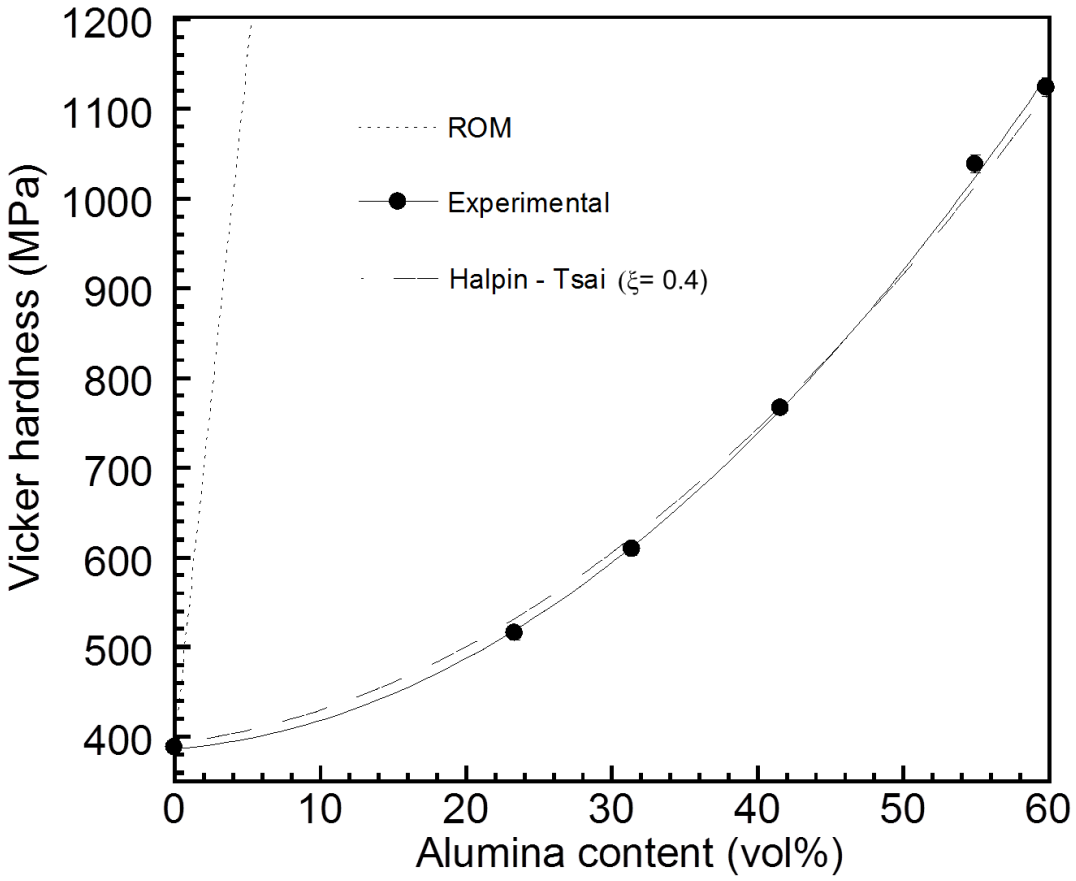

Figure 5.15 Relation between alumina content and the hardness of alumina filled polybenzoxazine composites.

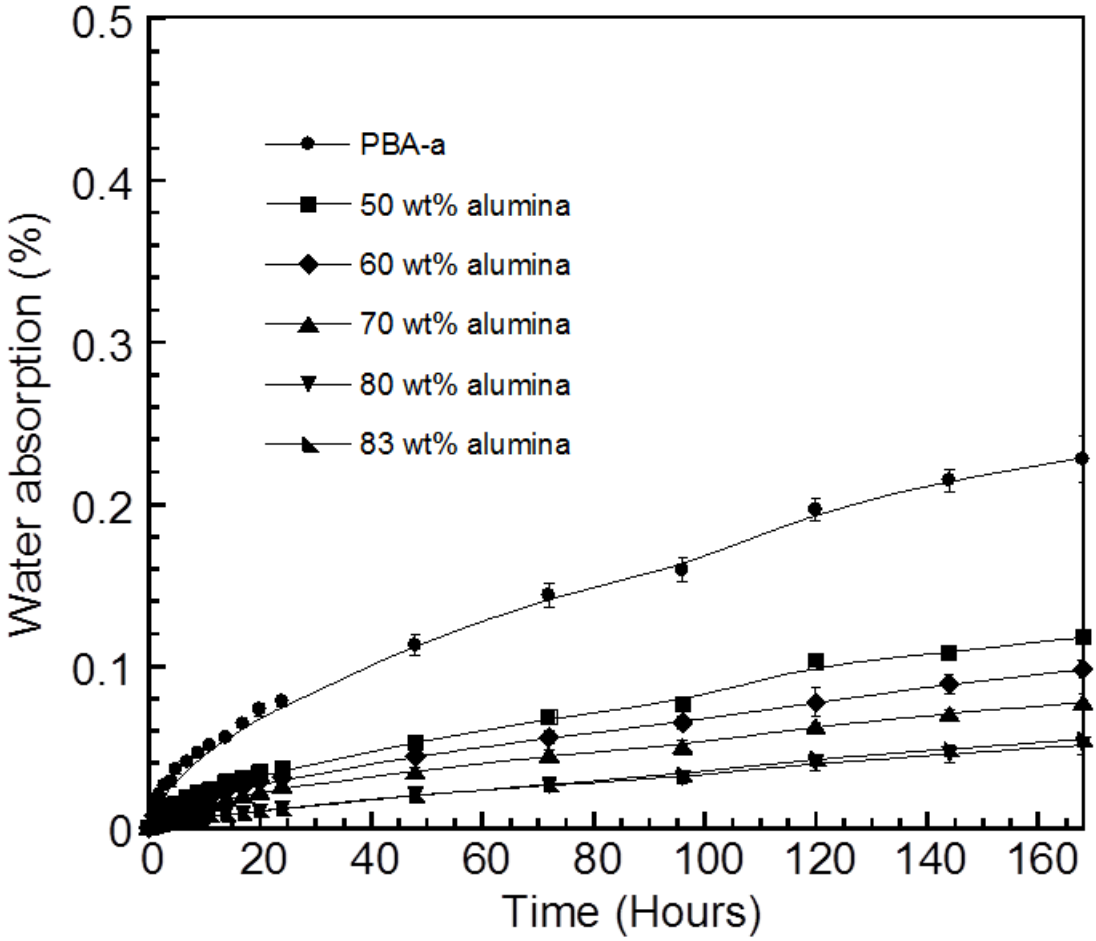

Figure 5.16 Water absorption of alumina filled polybenzoxazine composites at various alumina contents: (●) neat polybenzoxazine (■) 50wt%, (♦) 60wt%, (▲) 70wt%, (▼) 80wt%, (◣) 83wt%.

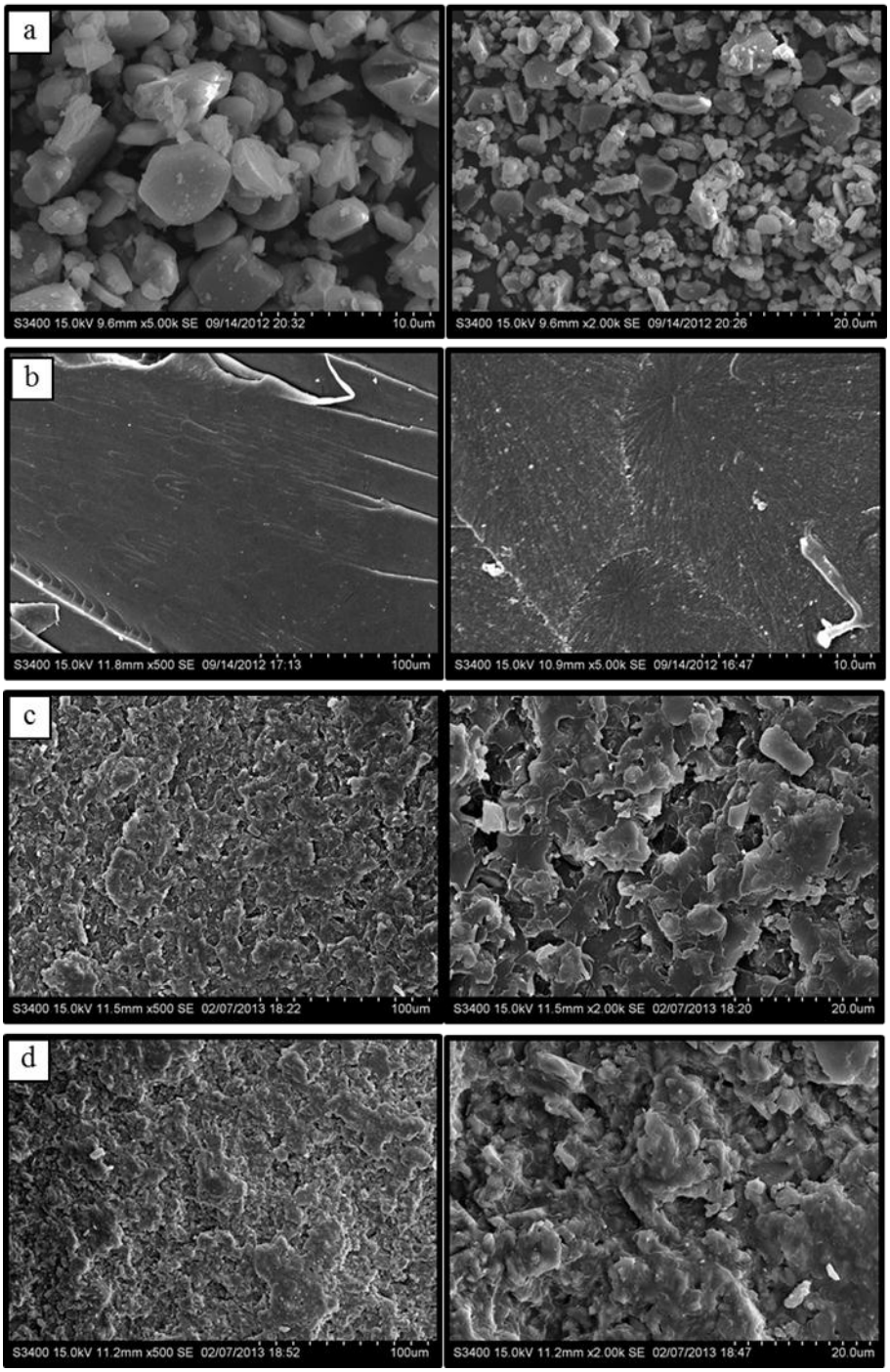

Figure 5.17 SEM micrographs of fracture surface of alumina-filled polybenzoxazine composites: (a) pure alumina, (b) neat polybenzoxazine (PBA-a), (c) 50wt% alumina-filled PBA-a, (d) 83wt% alumina-filled PBA-a

Table5.4 Properties comparison of alumina and glass fiber composites.

Composites	20/80:BA-a/Alumina(1)	20/80:BA-a/Alumina(2)	100/0:glass(1)	100/0:glass(2)
Areal weight	2.66	2.64	0.62	0.55
Striking velocity (m/s)	339.9	338.7	342.4	343.7
Residual velocity (m/s)	102.4	56.1	301.2	310.3
Delta velocity (m/s)	237.5	282.6	41.3	33.4
Impact energy (J)	711.10	705.92	721.56	727.09
Residual energy (J)	64.56	19.36	558.18	592.59
Absorbed energy (J)	646.54	686.56	163.38	134.50
Absorbed energy/areal weight	242.64	259.88	265.00	244.82
Absorbed energy/thickness	64.65	68.66	51.87	45.59

CHAPTER VI

CONCLUSIONS

Highly filled systems of alumina filled polybenzoxazine composites with the maximum alumina content of 83wt% (60vol%) were achieved in this work. The composites exhibit properties highly suitable for wear resistance and electronic applications.

The DSC experiment revealed that the optimal curing condition to obtain the fully-cured specimens of the alumina-filled polybenzoxazine composites was by heating at 200^{o}C for 2 hours in a hydraulic hot-pressed machine at 15 MPa. The mechanical and thermal properties of alumina-filled polybenzoxazine composites at different alumina contents in the range 0 to 83 wt% tended to increase with increasing alumina contents. The actual density of the composites was measured to be close to the theoretical one suggesting negligible amount of void was presented in the composites. The glass transition temperature of alumina filled polybenzoxazine was found to increase with increasing the alumina contents. The degradation temperatures (at 5% weight loss under nitrogen atmosphere) and solid residue (at 800^{o}C) of the composites were also observed to substantially increase with increasing the alumina contents.

In addition, the modulus of the highly filled polybenzoxazine composites was significantly improved by the presence of the alumina even at only few percent of the filler. The flexural strength increased with increasing alumina contents. Furthermore, the hardness of alumina filled polybenzoxazine composites significantly increased with increasing alumina contents. The storage modulus of the composite also exhibited the similar trend with the flexural modulus. Additionally, water absorption of the composites was significantly suppressed by the addition of the alumina-filler. Moreover, ballistic performance, the absorbed energy of alumina composites was similar to glass fiber composites. Finally, Scanning electron micrographs revealed

good filler-matrix interfacial adhesion with tight interfaces between the alumina and the polybenzoxazine matrix.

REFERENCES

[1] A. Krell, J. Klimke and T. Hutzler. Advanced spinel and sub-μm Al_2O_3 for transparent armour applications. J. Eur Ceram Soc. 29(2009): 275.

[2] C.A. Harper. Handbook of ceramics glasses and diamonds. McGraw-Hill: New York, 1976.

[3] L. Kloc, P. Marecek and J. Fiala. Creep of Zr-doped alumina at very low creep rates. Mater. Sci. Eng. A. 64(2004): 1551.

[4] K.R. Ahmad, S.B. Jamaludin, L.B. Hussain and Z.A. Ahmad. The influence of alumina particle size on sintered density and hardness of discontinuous reinforced aluminum metal matrix composite. J. Teknologi. 42(2005): 49.

[5] H. Majidian, T. Ebadzadeh and E. Salahi. Effect of SiC additions on microstructure, mechanical properties and thermal shock behavior of alumina-mullite-zirconia composites. Mater. Sci. Eng. A. 530(2011): 585.

[6] H. F. Mark, N. G. Gaylord and N. M. Bikales. Encyclopedia of polymer science and engineer. 16th edition. John Wiley & Sons: New York, 1972.

[7] N. N. Ghosh, B. Kiskan and Y. Yagci. Polybenzoxazines-new high performance thermosetting resins: synthesis and properties. Prog. Polym. Sci. 32(2007): 1344.

[8] C. P. R. Nair. Advances in addition-cure phenolic resins. Prog. Polym. Sci. 29(2004): 401.

[9] M. A. Espinosa, V. Cadiz and M. Galia. Synthesis and characterization of benzoxazine-based phenolic resins: crosslinking study. J. Appl. Polym. Sci. 90(2003): 470.

[10] H. Ishida. Process for preparation of benzoxazine compounds in solventless systems. U.S. Patent 5,543,516 (1996).

[11] H. Ishida and D. J. Allen. Physical and mechanical characterization of near-zero shrinkage polybenzoxazines. J. Polym. Sci. Pol. Phys. 34(1996): 1019.

[12] R. M. German. Particle packing characteristics. Metal Powder: New Jersey, 1989.

[13] B. Venkatesulu and M. J. Thomas. Erosion resistance of alumina-filled silicone rubber nanocomposites. IEEE. T. Dielect. El. In. 17(2010): 2.

[14] M. Fasihi and H. Garmabi. Evaluation and optimization of the mechanical properties of highly filled PVC/(wood flour) composites by using experimental design. J. Vinyl. Addit. Techn. 17(2011): 112.

[15] T. Kaully, A. Siegmann and D. Shacham. Mechanical behavior of highly filled natural $CaCO_3$ composites: effect of particle size distribution and interface interactions. Polym. Composite. 29(2008): 394.

[16] R. A. Hauser, J. A. King, R. M. Pagel and J. M. Keith. Effects of carbon fillers on the thermal conductivity of highly filled liquid-crystal polymer based resins. J. Appl. Polym. Sci. 109(2008): 2145.

[17] Ling Du and S. C. Jana. Highly conductive epoxy/graphite composites for bipolar plates in proton exchange membrane fuel cells. J. Power. Sources. 172(2007): 734.

[18] B. Pick, M. Pelka, R Belli, R. R. Braga and U Lohbauer. Tailoring of physical properties in highly filled experimental nanohybrid resin composites. Dent. Mater. 27(2011): 664.

[19] Z. Li, H. Gao and Q. Wang. Preparation of highly filled wood flour/recycled high density polyethylene composites by in situ reactive extrusion. J. Appl. Polym. Sci. 124(2012): 5247.

[20] S. Rimdusit, W. Tanthapanichakoon and C. Jubsilp. High performance wood composites from highly filled polybenzoxazine. J. Appl. Polym. Sci. 99(2006): 1240.

[21] M. Bengtsson, M. L. Baillif and K. Oksman. Extrusion and mechanical properties of highly filled cellulose fiber–polypropylene composites. Compos. Part A. 38(2007): 1922.

[22] H. Ishida and S. Rimdusit. Very high thermal conductivity obtained by boron nitride-filled polybenzoxazine. Thermochim. Acta. 320(1998): 177.

[23] H. Ishida. Composition for forming high thermal conductivity polybenzoxazine-based material and method. U.S. Patent 5,900,447 (1999).

[24] H. Zhang, H. Zhang, L. Tang, Z. Zhang, L. Gu, Y. Xu and C. Eger. Wear-resistant and transparent acrylate-based coating with highly filled nanosilica particles. Tribol. Int. 43(2010): 83.

[25] J. Abenojar, M. A. Martinez, F. Velasco, V. Pascual-Sanchez and J. M. Martin-Martinez. Effect of boron carbide filler on the curing and mechanical properties of an epoxy resin. J. Adhesion. 85(2009): 216.

[26] T. Kauly, B. Kecren and A. Siegmann. Highly filled thermoplastic composites. II: effects of particle size distribution on some properties. Polym. Composite. 17(1996): 6.

[27] R. M. German. Power metallurgy science. 2nd edition. Metal Powder: New Jersey, 1994.

[28] R. N. Rothon. Particulate-filled polymer composites. 2nd Edition. Smithers Rapra Technology: Shrewsbury, 2003.

[29] H. Ishida and D. J. Allen. Mechanical characterization of copolymers based on benzoxazine and epoxy. Polymer. 37(1996): 4487.

[31] K. Davis. Material review: alumina (Al_2O_3). School of doctoral studies (European union) journal. (2010): 109.

[32] E. Medvedovski. Ballistic performance of armour ceramics: Influence of design and structure Part 1. Ceram. Int. 36(2010): 2103.

[33] N. Suprapakorn, S. Dhamrongvaraporn and H. Ishida. Effect of $CaCO_3$ on the mechanical and rheological properties of a ring – opening phenolic resin: polybenzoxazine. Polym. Composite. 19(1998): 2.

[34] L. M. McGrath, R. S. Parnas, S. H. King, J. L. Schroeder, D. A. Fischer and J. L. Lenhart. Investigation of the thermal, mechanical and fracture properties of alumina – epoxy composites. Polymer. 49(2008): 999.

[35] S. Rimdusit and H. Ishida. Development of new class of electronic packaging materials based on ternary systems of benzoxazine, epoxy, and phenolics resins Polymer. 41(2000): 7941.

[36] P. Kasemsiri, S. Hiziroglu and S. Rimdusit. Effect of cashew nut shell liquid on gelation, cure kinetics, and thermomechanical properties of benzoxazine resin. Thermochim. Acta. 520(2011): 84.

[37] B. S. Rao and A. Palanisamy. Monofunctional benzoxazine from cardanol for bio-composite applications. React. Funct. Polym. 71(2011): 148.

[38] C. Jubsilp, T. Takeichi, and S. Rimdusit. Polymerization kinetics. Handbook of benzoxazine resins. Chapter **7**(2011): 157.

[39] C. P. Wong and R. S. Bollampally. Thermal Conductivity, elastic modulus, and coefficient of thermal expansion of polymer composites filled with Ceramic particles for electronic packaging. J. Appl. Polym. Sci. 74(1999): 3396.

[40] R.K. Goyal, A. N. Tiwari and Y. S. Negi. Role of interface on dynamic modulus of high – performance poly(etheretherketone)/ceramic composites. J. Appl. Polym. Sci. 121(2011): 436.

[41] I. H. Tavman. Thermal and mechanical properties of copper powder filled poly (ethylene) composites. Power Technol. 91(1997): 63.

[42] E. Vassileva and K. Friedrich. Epoxy/alumina nanoparticle composites. I. Dynamic mechanical behavior. J. Appl. Polym. Sci. 89(2003): 3774.

[43] G. C. Papanicolaou, A. G. Xepapadaki, A. Kotrotsos and D. E. Mouzakis. Interphase modeling of copper-epoxy particulate composites subjected to static and dynamic loading. J. Appl. Polym. Sci. 109(2008): 1150.

[44] L. E. Nielsen and R. F. Landel. Mechanical Properties of Polymers and Composites. Marcel Dekker: New York, 1994.

[45] I. Hamerton, B. J. Howlin, A. L. Mitchell, S. A. Hall, and L. McNamara. Using molecular simulation to predict the physical and mechanical properties of polybenzoxazines. Handbook of benzoxazine resins. Chapter 5(2011): 137.

[46] M. Hhssain, A. Nakahira, S. Nishijima and K. Niihara. Effects of coupling agents on the mechanical properties improvement of the TiO_2 reinforced epoxy system. Mater Lett. 26(1996): 299.

[47] M. Kaleemullah, S. U. Khan and J-K. Kim. Effect of surfactant treatment on thermal stability and mechanical properties of CNT/polybenzoxazine nanocomposites. Compos. Sci. Technol. 72(2012): 1968.

[48] T. Takeichi, R. Zeidam and T. Agag. Polybenzoxazine/clay hybrid nanocomposites: influence of preparation method on the curing behavior and properties of polybenzoxazines. Polymer. 43(2002): 45.

[49] S. Hemsri, A. D. Asandei, K. Grieco and R. S. Parnas. Biopolymer composites of wheat gluten with silica and alumina. Compos. Part A. 42(2011): 1764.

[50] C. Jubsilp, T. Takeichi and S. Rimdusit. Effect of novel benzoxazine reactive diluent on processability and thermomechanical characteristics of bi-functional polybenzoxazine. J. Appl. Polym. Sci. 104(2007): 2928.

[51] S. Tiptipakorn, S. Damrongsakkul, S. Ando, K. Hemvichian and S. Rimdusit. Thermal degradation behaviors of polybenzoxazine and silicon-containing polyimide blends. Polym. Degrad. Stabil. 92(2007): 1265.

[52] S. Rimdusit, S. Pirstpindvong, W. Tanthapanichakoon and S. Damrongsakkul. Toughening of polybenzoxazine by alloying with urethane prepolymer and flexible epoxy: a comparative study. Polym. Eng. Sci. 45(2005): 288.

[53] S. Rimdusit, N. Kampangsaeree, W. Tanthapanichakoon, T. Takeichi and N. Suppakarn. Development of wood-substituted composites from highly filled polybenzoxazine-phenolic novolac alloys. Polym. Eng. Sci. 47(2007): 140.

[54] S. Rimdusit, P. Jongvisuttisun, C. Jubsilp and W. Tanthapanichakoon. Highly processable ternary systems based on benzoxazine, epoxy, and phenolic resins for carbon fiber composite processing. J. Appl. Polym. Sci. 111(2009): 1225.

[55] C. Jubsilp, T. Takeichi and S. Rimdusit. Property enhancement of polybenzoxazine modified with dianhydride. Polym. Degrad. Stabil. 96(2011): 1047.

[56] S. Rimdusit, P. Kunopast and I. Dueramae. Thermomechanical properties of arylamine-Based benzoxazine resins alloyed with epoxy resin. Polym. Eng. Sci. 51(2011): 1797.

[57] A. Yasmin and I. M. Daniel. Mechanical and thermal properties of graphite/epoxy composites. Polymer. 45(2004): 8211.

[58] X. Zhang, W. Xu, X. Xia, Z. Zhang and R. Yu. Toughening of cycloaliphatic epoxy resin by nanosize silicon dioxide. Mater Lett. 60(2006): 3319.

[59] E. S. A. Rashid, K. Ariffin and H. M. Akil. Mechanical and thermal properties of polymer composites for electronic packaging application. J. Reinf. Plast. Comp. 27(2008): 15.

[60] S-Y. Fu, X-Q. Feng, B. Lauke and Y-W. Mai. Effects of particle size, particle/matrix interface adhesion and particle loading on mechanical properties of particulate–polymer composites. Composites: Part B. 39(2008): 933.

[61] P. Kasemsiri, S. Hiziroglu and S. Rimdusit. Properties of wood polymer composites from eastern redcedar particles reinforced with benzoxazine resin/cashew nut shell liquid copolymer. Compos. Part A. 42(2011): 1454.

[62] G. Yi and F. Yan. Mechanical and tribological properties of phenolic resin-based friction composites filled with several inorganic fillers. Wear. 262(2007): 121.

[63] T.Oungkulsolmonglok, P. Salee-art and W. Buggakupta. Hardness and fracture toughness of alumina-based particulate composites with zirconia and strontia additives. Journal of Metals, Materials and Minerals. 20(2012): 71.

[64] M. Emamy, N. Nemati and A. Heidarzadeh. The influence of Cu rich intermetallic phases on the microstructure, hardness and tensile properties of Al-15%Mg_2Si composite. Mater. Sci. Eng. A. 527(2010): 2998.

[65] Y. K. Choi, K. I. Sugimoto, S. M. Song and M. Endo. Mechanical and thermal properties of vapor-grown carbon nanofiber and polycarbonate composite sheets. Mater Lett. 59(2005): 3514.

[66] R.K. Goyal, A.N. Tiwari and Y.S. Negi. Microhardness of PEEK/ceramic micro- and nanocomposites: Correlation with Halpin–Tsai model. Mater. Sci. Eng. A. 491(2008): 230.

[67] S. K. Sinha, T. Song, X. Wan and Y. Tong. Scratch and normal hardness characteristics of polyamide 6/nano-clay composite. Wear. 266(2009): 814.

[68] A. Allahverdi, M. Ehsani, H. Janpour and S. Ahmadi. The effect of nanosilica on mechanical, thermal and morphological properties of epoxy coating. Prog. Org. Coat. 75(2012): 543.

[69] H. Ishida. Overview and historical background of polybenzoxazine research. Handbook of benzoxazine resins. Chapter 1(2011): 11.

[70] H. Zhao and R. K. Y. Li. Effect of water absorption on the mechanical and dielectric properties of nano-alumina filled epoxy nanocomposites. Compos. Part A. 39(2008): 602.

APPENDIX

Characteristics of Alumina Filled Polybenzoxazine Composites

Appendix 1 Maximum packing density of alumina filled benzoxazine resin composites.

Alumina content (wt%)	Alumina content (vol%)	Theoretical density (g/cm^3)	Actual density (g/cm^3)
0	0	1.190	1.200
50	23	1.824	1.823
60	31	2.041	2.043
70	42	2.317	2.322
80	56	2.680	2.679
83	60	2.812	2.813
85	63	2.907	2.697

Appendix 2 Storage modulus (E') at 35^{o}C and the glass transition temperature (Tg, loss modulus), of alumina filled polybezoxazine composites at various alumina contents which were determined from DMA.

Alumina content (wt%)	Alumina content (vol%)	Storage modulus (E') at 35^{o}C (GPa)	Glass transition temperature (^{o}C)
0	0	5.9	172
50	23	11.3	178
60	31	17.1	180
70	42	20.6	182
80	56	38.4	188
83	60	45.3	185

Appendix 3 Flexural properties of alumina filled polybenzoxazine composite at room temperature.

Alumina content (wt%)	Alumina content (vol%)	Flexural modulus (GPa)	Flexural strength (MPa)
0	0	5.2 ± 0.1	133 ± 2
50	23	10.8 ± 0.4	97 ± 1
60	31	13.6 ± 0.1	104 ± 3
70	42	16.9 ± 0.6	124 ± 6
80	56	26.3 ± 1.9	139 ± 8
83	60	36.4 ± 2.9	142 ± 5

Appendix 4 Hardness properties of alumina filled polybenzoxazine composite at room temperature.

Alumina content (wt%)	Alumina content (vol%)	Micro-hardness (MPa)
0	0	388 ± 9
50	23	515 ± 7
60	31	609 ± 7
70	42	766 ± 5
80	56	1038 ± 10
83	60	1124 ± 11

Appendix 5 Water absorption of alumina filled polybenzoxazine composites at various alumina contents.

Alumina content (wt%)	Alumina content (vol%)	24 hr (%)	7days (%)
0	0	0.078 ± 0.0031	0.228 ± 0.0142
50	23	0.036 ± 0.0016	0.118 ± 0.0033
60	31	0.031 ± 0.0032	0.098 ± 0.0056
70	42	0.026 ± 0.0025	0.078 ± 0.0047
80	56	0.012 ± 0.0022	0.051 ± 0.0062
83	60	0.012 ± 0.0005	0.055 ± 0.0013

VITAE

Mr. Jirawat Kajohnchaiyagual was born in Phitsanulok, Thailand. He graduated at high school level in 2006 from Janokrong School. He received the Bachelor's Degree of Engineering with a major in Chemical Engineering from the Faculty of Engineer, Ubonrajathani University, Thailand in 2010. After graduation, he furthers his study for a Master's Degree of Chemical Engineering at the Department of Chemical Engineering, Faculty of Engineering, Chulalongkorn University.

Some parts of this work were selected for oral presentations in 1) The Seventh International Conference on Materials Science and Technology which was held during June 7-8, 2012 at Swissotel Le Concerde, Bangkok, Thailand and 2) The Nineteenth International Conference on Regional Symposium on Chemical Engineering which was held during November 7-8, 2012 at Bali.